Advances in Mathematics 300 (2016) 390–450

Contents lists available at ScienceDirect

Advances in Mathematics

www.elsevier.com/locate/aim

Integrable cluster dynamics of directed networks and pentagram maps

Michael Gekhtman [a,*], Michael Shapiro [b], Serge Tabachnikov [c,d], Alek Vainshtein [e]

[a] *Department of Mathematics, University of Notre Dame, Notre Dame, IN 46556, USA*
[b] *Department of Mathematics, Michigan State University, East Lansing, MI 48823, USA*
[c] *Department of Mathematics, Pennsylvania State University, University Park, PA 16802, USA*
[d] *ICERM, Brown University, Providence, RI 02903, USA*
[e] *Department of Mathematics and Department of Computer Science, University of Haifa, Haifa, Mount Carmel 31905, Israel*

ARTICLE INFO

Article history:
Received 9 June 2014
Accepted 3 December 2014
Available online 30 March 2016

To the memory of Andrei Zelevinsky

Keywords:
Generalized pentagram maps
Liouville integrability
Cluster dynamics
Mutations
Networks on surfaces

ABSTRACT

The pentagram map was introduced by R. Schwartz more than 20 years ago. In 2009, V. Ovsienko, R. Schwartz and S. Tabachnikov established Liouville complete integrability of this discrete dynamical system. In 2011, M. Glick interpreted the pentagram map as a sequence of cluster transformations associated with a special quiver. Using compatibility of Poisson and cluster structures and Poisson geometry of directed networks on surfaces, we generalize Glick's construction to include the pentagram map into a family of discrete integrable maps and we give these maps geometric interpretations. The appendix relates the simplest of these discrete maps to the Toda lattice and its tri-Hamiltonian structure.

* Corresponding author.
E-mail addresses: mgekhtma@nd.edu (M. Gekhtman), mshapiro@math.msu.edu (M. Shapiro), tabachni@math.psu.edu (S. Tabachnikov), alek@cs.haifa.ac.il (A. Vainshtein).

http://dx.doi.org/10.1016/j.aim.2016.03.023
0001-8708/

Contents

1. Introduction

The pentagram map was introduced by R. Schwartz more than 20 years ago [36]. The map acts on plane polygons by drawing the "short" diagonals that connect second-nearest vertices of a polygon and forming a new polygon, whose vertices are their consecutive intersection points, see Fig. 1. The pentagram map commutes with projective transformations, and therefore acts on the projective equivalence classes of polygons in the projective plane.

In fact, the pentagram map acts on a larger class of *twisted polygons*. A twisted n-gon is an infinite sequence of points $V_i \in \mathbf{RP}^2$ such that $V_{i+n} = M(V_i)$ for all $i \in \mathbf{Z}$ and a fixed projective transformation M, called the monodromy. The projective group $\mathrm{PGL}(3, \mathbf{R})$ naturally acts on twisted polygons. A polygon is closed if the monodromy is the identity.

Denote by $\mathcal{P}_n$ the moduli space of projective equivalence classes of twisted n-gons, and by $\mathcal{C}_n$ its subspace consisting of closed polygons. Then $\mathcal{P}_n$ and $\mathcal{C}_n$ are varieties of dimensions $2n$ and $2n - 8$, respectively. Denote by $T : \mathcal{P}_n \to \mathcal{P}_n$ the pentagram map (the ith vertex of the image is the intersection of diagonals (V_i, V_{i+2}) and (V_{i+1}, V_{i+3})).

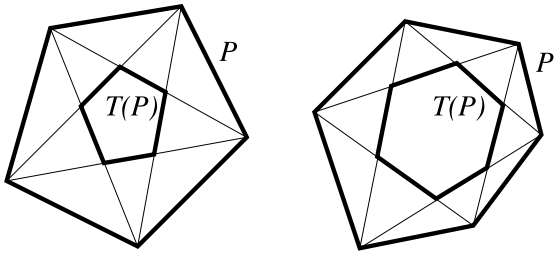

Fig. 1. Pentagram map.

One can introduce coordinates $X_1, Y_1, \dots, X_n, Y_n$ in $\mathcal{P}_n$ where X_i, Y_i are the so-called corner invariants associated with ith vertex, discrete versions of projective curvature, see [38]. In these coordinates, the pentagram map is a rational transformation

$$X_i^* = X_i \frac{1 - X_{i-1} Y_{i-1}}{1 - X_{i+1} Y_{i+1}}, \qquad Y_i^* = Y_{i+1} \frac{1 - X_{i+2} Y_{i+2}}{1 - X_i Y_i} \tag{1.1}$$

(the indices are taken mod n).

In [37], Schwartz proved that the pentagram map was recurrent, and in [38], he proved that the pentagram map had $2\lfloor n/2 \rfloor + 2$ independent integrals, polynomial in the variables X_i, Y_i. He conjectured that the pentagram map was a discrete completely integrable system.

This was proved in [31,32]: the space $\mathcal{P}_n$ has a T-invariant Poisson structure whose corank equals 2 or 4, according to whether n is odd or even, and the integrals are in involution. This provides Liouville integrability of the pentagram map on the space of twisted polygons.

F. Soloviev [42] established algebraic–geometric integrability of the pentagram map by constructing its Lax (zero curvature) representation. His approach established complete integrability of the pentagram map on the space of closed polygons $\mathcal{C}_n$ as well; a different proof of this result was given in [33].

It is worth mentioning that the continuous limit as $n \to \infty$ of the pentagram map is the Boussinesq equation, one of the best known completely integrable PDEs. More specifically, in the limit, a twisted polygon becomes a parametric curve (with monodromy) in the projective plane, and the map becomes a flow on the moduli space of projective equivalence classes of such curves. This flow is identified with the Boussinesq equation, see [36,32]. Thus the pentagram map is a discretization, both space- and time-wise, of the Boussinesq equation.

R. Schwartz and S. Tabachnikov discovered several configuration theorems of projective geometry related to the pentagram map in [40] and found identities between the integrals of the pentagram map on polygons inscribed into a conic in [41]. R. Schwartz [39] proved that the integrals of the pentagram map do not change in the 1-parameter family of Poncelet polygons (polygons inscribed into a conic and circumscribed about a conic).

It was shown in [38] that the pentagram map was intimately related to the so-called octahedral recurrence (also known as the discrete Hirota equation), and it was conjectured in [31,32] that the pentagram map was related to cluster transformations. This relation was discovered and explored by Glick [16] who proved that the pentagram map, acting on the quotient space $\mathcal{P}_n/\mathbf{R}^*$ (the action of $\mathbf{R}^*$ commutes with the map and is given by the formula $X_i \mapsto tX_i$, $Y_i \mapsto t^{-1}Y_i$), is described by coefficient dynamics [10] – also known as τ-transformations, see Chapter 4 in [13] – for a certain cluster structure.

In this paper, expanding on the research announcement [11], we generalize Glick's work by including the pentagram map into a family of discrete completely integrable systems. Our main tool is Poisson geometry of weighted directed networks on surfaces. The ingredients necessary for complete integrability – invariant Poisson brackets, integrals of motion in involution, Lax representation – are recovered from combinatorics of the networks.

A. Postnikov [34] introduced such networks in the case of a disk and investigated their transformations and their relation to cluster transformations; most of his results are local, and hence remain valid for networks on any surface. Poisson properties of weighted directed networks in a disk and their relation to r-matrix structures on GL_n are studied in [12]. In [15] these results were further extended to networks in an annulus and r-matrix Poisson structures on matrix-valued rational functions. Applications of these techniques to the study of integrable systems can be found in [14]. A detailed presentation of the theory of weighted directed networks from a cluster algebra perspective can be found in Chapters 8–10 of [13].

Our integrable systems, T_k, depend on one discrete parameter $k \geq 2$. The geometric meaning of $k-1$ is the dimension of the ambient projective space. The case $k = 3$ corresponds to the pentagram map, acting on planar polygons.

For $k \geq 4$, we interpret T_k as a transformation of a class of twisted polygons in $\mathbf{RP}^{k-1}$, called *corrugated polygons*. The map is given by intersecting consecutive diagonals of combinatorial length $k-1$ (i.e., connecting vertex V_i with V_{i+k-1}); corrugated polygons are defined as the ones for which such consecutive diagonals are coplanar. The map T_k is closely related with a pentagram-like map in the plane, involving deeper diagonals of polygons.

For $k = 2$, we give a different geometric interpretation of our system: the map T_2 acts on pairs of twisted polygons in $\mathbf{RP}^1$ having the same monodromy (these polygons may be thought of as ideal polygons in the hyperbolic plane by identifying $\mathbf{RP}^1$ with the circle at infinity), and the action is given by an explicit construction that we call the *leapfrog* map whereby one polygon "jumps" over another, see a description in Section 5. If the ground field is $\mathbf{C}$, we interpret the map T_2 in terms of circle patterns studied by O. Schramm [35,4].

The pentagram map is coming of age, and we finish this introduction by briefly mentioning, in random order, some related work that appeared since our initial research announcement [11] was written.

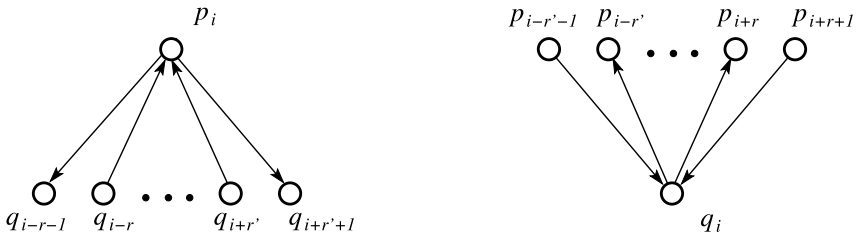

Fig. 2. The quiver $\mathcal{Q}_{k,n}$.

- A variety of multi-dimensional versions of the pentagram map, integrable and non-integrable, was studied by B. Khesin and F. Soloviev [22,23,25,24], and by G. Mari-Beffa [27,28]. The continuous limits of these maps are identified with the Adler–Gelfand–Dikii flows.
- V. Fock and A. Marshakov [9] described a class of integrable systems on Poisson submanifolds of the affine Poisson–Lie groups PGL(N). The pentagram map is a particular example. The quotient of the corresponding integrable system by the scaling action (see p-dynamics $\bar{T}_k$ defined in Section 2) coincides with the integrable system constructed by A. Goncharov and R. Kenyon out of dimer models on a two-dimensional torus and classified by the Newton polygons [19].
- M. Glick [17,18] established the singularity confinement property of the pentagram map and some other discrete dynamical systems.
- R. Kedem and P. Vichitkunakorn [21] interpreted the pentagram map in terms of T-systems.
- The pentagram map is amenable for tropicalization. A study of the tropical limit of the pentagram map was done by T. Kato [20].

2. Generalized Glick's quivers and the (p, q)-dynamics

For any integer $n \geq 2$, let $\mathbf{p} = (p_1, \dots, p_n)$ and $\mathbf{q} = (q_1, \dots, q_n)$ be independent variables. Fix an integer k, $2 \leq k \leq n$, and consider the quiver (an oriented multigraph without loops and cycles of length two) $\mathcal{Q}_{k,n}$ defined as follows: $\mathcal{Q}_{k,n}$ is a bipartite graph on $2n$ vertices labeled $p_1, \dots, p_n$ and $q_1, \dots, q_n$ (the labeling is cyclic, so that $n+1$ is the same as 1). The graph is invariant under the shift $i \mapsto i+1$. Each vertex has two incoming and two outgoing edges. The number k is the "span" of the quiver, that is, the distance between two outgoing edges from a p-vertex, see Fig. 2 where $r = \lfloor k/2 \rfloor - 1$ and $r + r' = k - 2$ (in other words, $r' = r$ for k even and $r' = r+1$ for k odd). For $k = 3$, we have Glick's quiver [16].

Let us equip the $(\mathbf{p}, \mathbf{q})$-space with a Poisson structure $\{\cdot, \cdot\}_k$ as follows. Denote by $A = (a_{ij})$ the $2n \times 2n$ skew-adjacency matrix of $\mathcal{Q}_{k,n}$, assuming that the first n rows and columns correspond to p-vertices. Then we put $\{v_i, v_j\}_k = a_{ij} v_i v_j$, where $v_i = p_i$ for $1 \leq i \leq n$ and $v_i = q_{i-n}$ for $n+1 \leq i \leq 2n$.

Consider a transformation of the $(\mathbf{p}, \mathbf{q})$-space denoted by $\overline{T}_k$ and defined as follows (the new variables are marked by asterisk):

$$q_i^* = \frac{1}{p_{i+r-r'}}, \quad p_i^* = q_i \frac{(1+p_{i-r'-1})(1+p_{i+r+1})p_{i-r'}p_{i+r}}{(1+p_{i-r'})(1+p_{i+r})}. \tag{2.1}$$

Theorem 2.1. (i) *The Poisson structure $\{\cdot,\cdot\}_k$ is invariant under the map $\overline{T}_k$.*

(ii) *The function $\prod_{i=1}^n p_i q_i$ is an integral of the map $\overline{T}_k$. Besides, it is Casimir, and hence the Poisson structure and the map descend to level hypersurfaces of $\prod_{i=1}^n p_i q_i$.*

Proof. (i) Recall that given an arbitrary quiver $\mathcal{Q}$, its *mutation* at vertex v is defined as follows:

1) for any pair of edges $u' \to v$, $v \to u''$ in $\mathcal{Q}$, the edge $u' \to u''$ is added;
2) all edges incident to v reverse their direction;
3) all cycles of length two are erased.

The obtained quiver is said to be *mutationally equivalent* to the initial one. Assume that an independent variable τ_v is assigned to each vertex of $\mathcal{Q}$. According to Lemma 4.4 of [13], the cluster transformation of τ-coordinates corresponding to the quiver mutation at vertex v (also known as cluster Y-dynamics) is defined as follows:

$$\tau_v^* = \frac{1}{\tau_v}, \qquad \tau_u^* = \begin{cases} \tau_u(1+\tau_v)^{\#(u,v)} & \text{if } \#(u,v) > 0, \\ \tau_u \frac{\tau_v^{\#(v,u)}}{(1+\tau_v)^{\#(v,u)}} & \text{if } \#(v,u) > 0, \\ \tau_u & \text{otherwise,} \end{cases} \tag{2.2}$$

where $\#(u', u'')$ is the number of edges from u' to u'' in $\mathcal{Q}$. Note that at most one of the numbers $\#(u,v)$ and $\#(v,u)$ is nonzero for any vertex u. The cluster structure associated with the initial quiver $\mathcal{Q}$ and initial set of variables $\{\tau_v\}_{v\in\mathcal{Q}}$ consists of all quivers mutationally equivalent to $\mathcal{Q}$ and of the corresponding sets of variables obtained by repeated application of (2.2).

Consider the cluster structure associated with the quiver $\mathcal{Q}_{k,n}$. Choose variables $\mathbf{p} = (p_1, \dots, p_n)$ and $\mathbf{q} = (q_1, \dots, q_n)$ as τ-coordinates, and consider cluster transformations corresponding to the quiver mutations at the p-vertices. These transformations commute, and we perform them simultaneously. By (2.2), this leads to the transformation

$$p_i^* = \frac{1}{p_i}, \quad q_i^* = q_i \frac{(1+p_{i-r'-1})(1+p_{i+r+1})p_{i-r'}p_{i+r}}{(1+p_{i-r'})(1+p_{i+r})}. \tag{2.3}$$

The resulting quiver is identical to $\mathcal{Q}_{k,n}$ with the letters p and q interchanged. Indeed, the mutation at p_i generates four new edges $q_{i-r} \to q_{i+r'+1}$, $q_{i+r'} \to q_{i+r'+1}$, $q_{i-r} \to q_{i-r-1}$, and $q_{i+r'} \to q_{i-r-1}$. The first of them disappears after the mutation at p_{i+1}, the second after the mutation at p_{i+k-1}, the third after the mutation at p_{i-k+1}, and the

fourth after the mutation at p_{i-1}. Therefore, the result of mutations at all p-vertices is just the reversal of all edges of $\mathcal{Q}_{k,n}$. Thus we compose transformation (2.3) with the transformation given by $\bar{p}_i = q_i$, $\bar{q}_i = p_{i+r-r'}$ and arrive at the transformation $\overline{T}_k$ defined by (2.1). The difference in the formulas for the odd and even k is due to the asymmetry between left and right in the enumeration of vertices in Fig. 2 for odd k, when $r' \neq r$.

A Poisson structure $\{\cdot,\cdot\}$ is said to be compatible with a cluster structure if $\{x_i, x_j\} = c_{ij} x_i x_j$ for any two variables from the same cluster, where the constants c_{ij} depend on the cluster (the cluster basis is related to the τ-basis described above via monomial transformations; we will not need the explicit description of these transformations here). By Theorem 4.5 in [13], the Poisson structure $\{\cdot,\cdot\}_k$ is compatible with the above cluster structure. Consequently, $\{\cdot,\cdot\}_k$ can be written in the basis (2.3) in the same way as above via the adjacency matrix of the resulting quiver. After the vertices are renamed, we arrive back at $\mathcal{Q}_{k,n}$, which means that $\{\cdot,\cdot\}_k$ is invariant under $\overline{T}_k$.

(ii) Invariance of the function $\prod_{i=1}^n p_i q_i$ means the equality $\prod_{i=1}^n p_i^* q_i^* = \prod_{i=1}^n p_i q_i$, which is checked directly by inspection of formulas (2.1). The statement that $\prod_{i=1}^n p_i q_i$ is Casimir (or, equivalently, commutes with any p_i and q_i) follows from the form of the quiver, since every vertex has an equal number (2, exactly) of incoming and outgoing edges. Hence, the level hypersurface $\prod_{i=1}^n p_i q_i = \text{const}$ is a Poisson submanifold, and, moreover, $\overline{T}_k$ preserves the hypersurface. □

Along with the p-dynamics $\overline{T}_k$, when the mutations are performed at the p-vertices of the quiver $\mathcal{Q}_{k,n}$, one may consider the respective q-dynamics $\overline{T}_k^\circ$, when the mutations are performed at q-vertices. Let us define an auxiliary map $\overline{D}_k$ given by

$$\bar{p}_i = \frac{1}{q_i}, \qquad \bar{q}_i = \frac{1}{p_{i+r-r'}}. \tag{2.4}$$

Note that $\overline{D}_k$ is almost an involution: $\overline{D}_k^2 = S_{r-r'}$, where S_t is the shift by t in indices. The following proposition describes relations between transformations $\overline{T}$, $\overline{T}^{-1}$, and $\overline{T}^\circ$.

Proposition 2.2. (i) *Transformation $\overline{T}_k^\circ$ coincides with $\overline{T}_k^{-1}$ and is given by*

$$p_i^* = \frac{1}{q_{i-r+r'}}, \quad q_i^* = p_i \frac{(1+q_{i-r})(1+q_{i+r'})q_{i-r-1}q_{i+r'+1}}{(1+q_{i-r-1})(1+q_{i+r'+1})}. \tag{2.5}$$

(ii) *Transformations $\overline{T}_k^\circ$ and $\overline{T}_k$ are almost conjugated by $\overline{D}_k$:*

$$S_{r-r'} \circ \overline{T}_k^\circ \circ \overline{D}_k = \overline{D}_k \circ \overline{T}_k. \tag{2.6}$$

(iii) *Let $\overline{D}_{k,n}$ be given by $\bar{p}_i = q_{i-\lfloor (n+r-r')/2 \rfloor}$, $\bar{q}_i = p_i$. Then*

$$\overline{T}_k^\circ = \overline{D}_{k,n} \circ \overline{T}_{n+2-k} \circ \overline{D}_{k,n}.$$

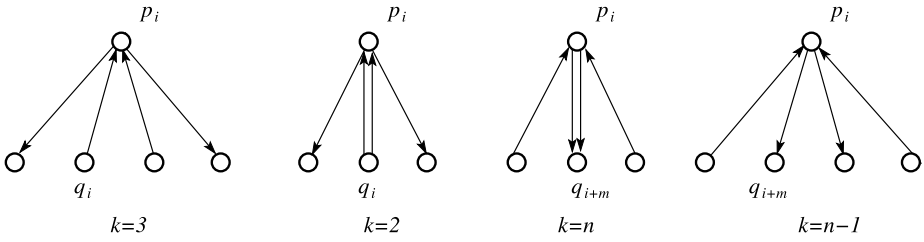

Fig. 3. The quivers $\mathcal{Q}_{k,n}$ for $n = 2m$ and various values of k.

Proof. (i) Recall that $\overline{T}_k$ is defined as the composition of the cluster transformation (2.3) and the shift $\bar{p}_i = q_i$, $\bar{q}_i = p_{i+r-r'}$ Equivalently, we can write $\overline{T}_k = \overline{C}_k \circ \overline{D}_k$, where $\overline{C}_k$ is given by expressions reciprocal to those in the right-hand side of (2.3). It is easy to check that $\overline{C}_k$ is an involution, and that $\overline{D}_k^{-1} = S_{r'-r} \circ \overline{D}_k$ is given by $\bar{p}_i = 1/q_{i-r+r'}$, $\bar{q}_i = 1/p_i$. Consequently, $\overline{T}_k^{-1} = \overline{D}_k^{-1} \circ \overline{C}_k$ is given by (2.5).

To get the same relations for the transformation $\overline{T}_k^{\circ}$ one has to use an analog of (2.3)

$$q_i^* = \frac{1}{q_i}, \quad p_i^* = p_i \frac{(1+q_{i-r})(1+q_{i+r'})q_{i-r-1}q_{i+r'+1}}{(1+q_{i-r-1})(1+q_{i+r'+1})}$$

and compose it with the map $\bar{q}_i = p_i$, $\bar{p}_i = q_{i-r+r'}$, see Fig. 2.

(ii) Follows immediately from (i).

(iii) Follows from the fact that $\mathcal{Q}_{n+2-k,n}$ locally at the vertex $q_{i+\lfloor (n+r-r')/2 \rfloor}$ has the same structure as $\mathcal{Q}_{k,n}$ at the vertex p_i. This is illustrated in Fig. 3.

For a formal proof note that the values $\hat{r}$ and $\hat{r}'$ corresponding to $\hat{k} = n + 2 - k$ are given by

$$\hat{r} = \lfloor (n + r - r')/2 \rfloor - r - 1, \qquad \hat{r} + \hat{r}' = n - k. \qquad \square \tag{2.7}$$

By Theorem 2.1(ii), $\overline{T}_k$ restricts to any hypersurface $\prod_{i=1}^n p_i q_i = c$. We denote this restriction by $\overline{T}_k^{(c)}$. In what follows, we shall be concerned only with $\overline{T}_k^{(1)}$. Note that $\overline{T}_3^{(1)}$ is the pentagram map on $\mathcal{P}_n/\mathbf{R}^*$ considered by Glick [16].

3. Weighted directed networks and the (x, y)-dynamics

3.1. Weighted directed networks on surfaces

We start with a very brief description of the theory of weighted directed networks on surfaces with a boundary, adapted for our purposes; see [34,13] for details. In this paper, we will only need to consider graphs on a cylinder (equivalently, annulus) $\mathcal{C}$ that we position horizontally with one boundary circle on the left and another on the right.

Let G be a directed graph with the vertex set V and the edge set E embedded in $\mathcal{C}$. G has $2n$ *boundary vertices*, each of degree one: n *sources* on the left boundary circles and n *sinks* on the right boundary circle. All the internal vertices of G have degree 3

and are of two types: either they have exactly one incoming edge (white vertices), or exactly one outgoing edge (black vertices). To each edge $e \in E$ we assign the *edge weight* $w_e \in \mathbf{R} \setminus 0$. A *perfect network* $\mathcal{N}$ is obtained from G by adding an oriented curve ρ without self-intersections (called a *cut*) that joins the left and the right boundary circles and does not contain vertices of G. The points of the *space of edge weights* $\mathcal{E}_{\mathcal{N}}$ can be considered as copies of $\mathcal{N}$ with edges weighted by nonzero real numbers.

Assign an independent variable λ to the cut ρ. The weight of a directed path P between a source and a sink is defined as a signed product of the weights of all edges along the path times λ^d, where d is the intersection index of ρ and P (we assume that all intersection points are transversal, in which case the intersection index is the number of intersection points counted with signs). The sign is defined by the rotation number of the loop formed by the path, the cut, and parts of the boundary cycles (see [15] for details). In particular, the sign of a simple path going from one boundary circle to the other one and intersecting the cut d times in the same direction equals $(-1)^d$. Besides, if a path P can be decomposed in a path P' and a simple cycle, then the signs of P and P' are opposite. The *boundary measurement* between a given source and a given sink is then defined as the sum of path weights over all (not necessary simple) paths between them. A boundary measurement is rational in the weights of edges and λ, see Proposition 2.2 in [15]; in particular, if the network does not have oriented cycles then the boundary measurements are polynomials in edge weights, λ and λ^{-1}.

Boundary measurements are organized in a *boundary measurement matrix*, thus giving rise to the *boundary measurement map* from $\mathcal{E}_{\mathcal{N}}$ to the space of $n \times n$ rational matrix functions. The gauge group acts on $\mathcal{E}_{\mathcal{N}}$ as follows: for any internal vertex v of $\mathcal{N}$ and any Laurent monomial L in the weights w_e of $\mathcal{N}$, the weights of all edges leaving v are multiplied by L, and the weights of all edges entering v are multiplied by L^{-1}. Clearly, the weights of paths between boundary vertices, and hence boundary measurements, are preserved under this action. Therefore, the boundary measurement map can be factorized through the space $\mathcal{F}_{\mathcal{N}}$ defined as the quotient of $\mathcal{E}_{\mathcal{N}}$ by the action of the gauge group.

It is explained in [15] that $\mathcal{F}_{\mathcal{N}}$ can be parametrized as follows. The graph G divides $\mathcal{C}$ into a finite number of connected components called *faces*. The boundary of each face consists of edges of G and, possibly, of several arcs of $\partial\mathcal{C}$. A face is called *bounded* if its boundary contains only edges of G and *unbounded* otherwise. Given a face f, we define its *face weight* $y_f = \prod_{e \in \partial f} w_e^{\gamma_e}$, where $\gamma_e = 1$ if the direction of e is compatible with the counterclockwise orientation of the boundary ∂f and $\gamma_e = -1$ otherwise. Face weights are invariant under the gauge group action. Then $\mathcal{F}_{\mathcal{N}}$ is parametrized by the collection of all face weights (subject to condition $\prod_f y_f = 1$) and a weight of an arbitrary path in G (not necessary directed) joining two boundary circles; such a path is called a *trail*.

Below we will frequently use elementary transformations of weighted networks that do not change the boundary measurement matrix. They were introduced by Postnikov in [34] and are presented in Fig. 4.

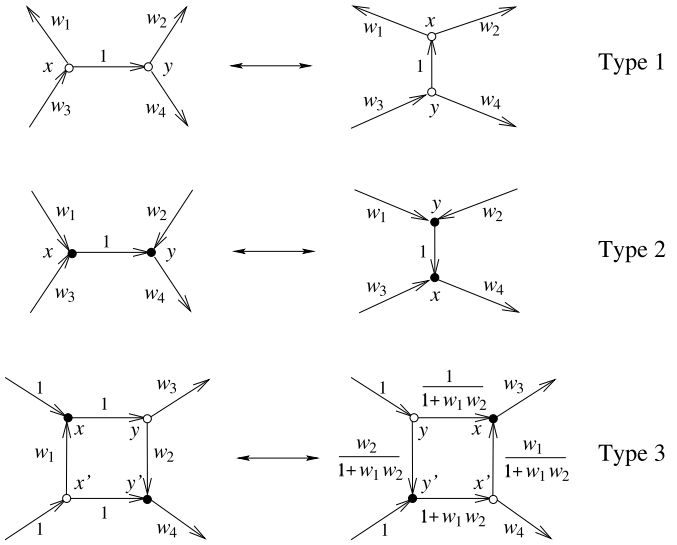

Fig. 4. Postnikov transformations.

Another important transformation is *path reversal*: for a given closed path one can reverse the directions of all its edges and replace each weight w_i with $1/w_i$. Clearly, path reversal preserves face weights. The transformations of boundary measurements under path reversal are described in [34,12,15].

As was shown in [12,15], the space of edge weights can be made into a Poisson manifold by considering Poisson brackets that behave nicely with respect to a natural operation of concatenation of networks. Such Poisson brackets on $\mathcal{E}_{\mathcal{N}}$ form a 6-parameter family, which is pushed forward to a 2-parameter family of Poisson brackets on $\mathcal{F}_{\mathcal{N}}$. Here we will need a specific member of the latter family. The corresponding Poisson structure, called *standard*, is described in terms of the *directed dual network* $\mathcal{N}^*$ defined as follows. Vertices of $\mathcal{N}^*$ are the faces of $\mathcal{N}$. Edges of $\mathcal{N}^*$ correspond to the edges of $\mathcal{N}$ that connect either two internal vertices of different colors, or an internal vertex with a boundary vertex; note that there might be several edges between the same pair of vertices in $\mathcal{N}^*$. An edge e^* in $\mathcal{N}^*$ corresponding to e in $\mathcal{N}$ is directed in such a way that the white endpoint of e (if it exists) lies to the left of e^* and the black endpoint of e (if it exists) lies to the right of e. The weight $w^*(e^*)$ equals 1 if both endpoints of e are internal vertices, and 1/2 if one of the endpoints of e is a boundary vertex. Then the restriction of the standard Poisson bracket on $\mathcal{F}_{\mathcal{N}}$ to the space of face weights is given by

$$\{y_f, y_{f'}\} = \left(\sum_{e^*: f \to f'} w^*(e^*) - \sum_{e^*: f' \to f} w^*(e^*) \right) y_f y_{f'}. \tag{3.1}$$

The bracket of the trail weight z and a face weight y_f is given by $\{z, y_f\} = c_f z y_f$. The description of c_f in the general case is rather lengthy. We will only need it in the case

when the trail is a directed path P in G. In this case

$$\{z, y_f\} = \sum_{P' \subset P} \pm \left(\sum_{e \in P', e^*: f \to f'} w^*(e^*) - \sum_{e \in P', e^*: f' \to f} w^*(e^*) \right) z y_f, \tag{3.2}$$

where each P' is a maximal subpath of P that belongs to ∂f, and the sign before the internal sum is positive if f lies to the right of P' and negative otherwise.

Any network $\mathcal{N}$ of the kind described above gives rise to a network $\bar{\mathcal{N}}$ on a torus. To this end, one identifies boundary circles in such a way that the endpoints of the cut are glued together, and the ith source in the clockwise direction from the endpoint of the cut is glued to the ith sink in the clockwise direction from the opposite endpoint of the cut. The resulting two-valent vertices are then erased, so that every pair of glued edges becomes a new edge with the weight equal to the product of two edge-weights involved. Similarly, n pairs of unbounded faces are glued together into n new faces, whose face-weights are products of pairs of face-weights involved. We will view two networks on a torus as *equivalent* if their underlying graphs differ only by orientation of edges, but have the same vertex coloring and the same face weights. The parameter space we associate with $\bar{\mathcal{N}}$ consists of face weights and the weights z_ρ, z of two trails P_ρ and P. The first of them is homological to the closed curve on the torus obtained by identifying endpoints of the cut, and the second is noncontractible and not homological to the first one. The standard Poisson bracket induces a Poisson bracket on face-weights of the new network, which is again given by (3.1) with the dual graph $\mathcal{N}^*$ replaced by $\bar{\mathcal{N}}^*$ defined by the same rules. The bracket between z_ρ or z and face-weights is given by (3.2), provided the corresponding trails are directed paths in G. Finally, under the same restriction on the trails,

$$\{z, z_\rho\} = \sum_{P'} c_{P'} z z_\rho, \tag{3.3}$$

where each P' is a maximal common subpath of P and P_ρ and $c_{P'}$ is defined in Fig. 5.

3.2. The $(\mathbf{x}, \mathbf{y})$*-dynamics*

Let us define a network $\mathcal{N}_{k,n}$ on the cylinder. It has k sources, k sinks, and $4n$ internal vertices, of which $2n$ are black, and $2n$ are white. $\mathcal{N}_{k,n}$ is glued of n isomorphic pieces, as shown in Fig. 6.

The pieces are glued together in such a way that the lower right edge of the ith piece is identified with the upper left edge of the $(i+1)$th piece, provided $i+1 \leq n$, and the upper right edge of the ith piece is identified with the lower left edge of the $(i+k-1)$st piece, provided $i+k-1 \leq n$. The network $\bar{\mathcal{N}}_{k,n}$ on the torus is obtained by dropping the latter restriction and considering cyclic labeling of pieces. The faces of $\bar{\mathcal{N}}_{k,n}$ are quadrilaterals and octagons. The cut hits only octagonal faces and intersects each white–white edge.

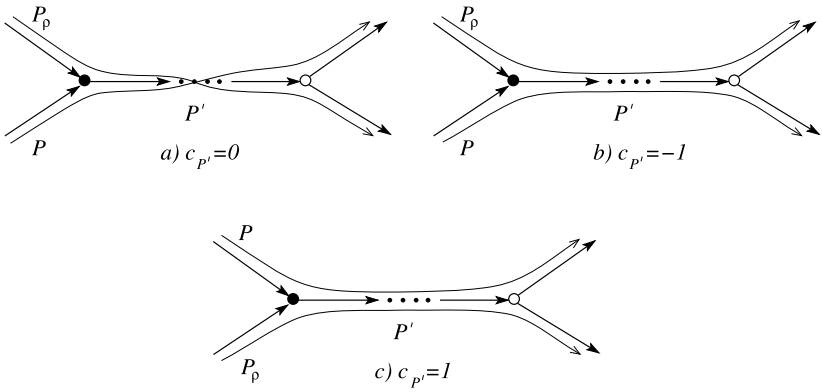

Fig. 5. To the definition of $c_{P'}$.

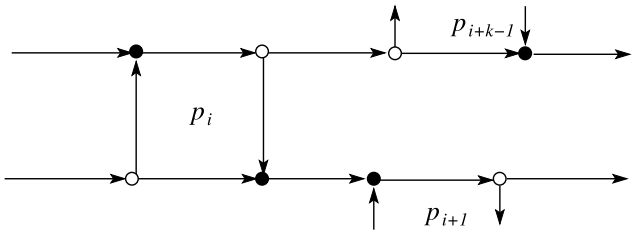

Fig. 6. Local structure of the networks $\mathcal{N}_{k,n}$ and $\bar{\mathcal{N}}_{k,n}$.

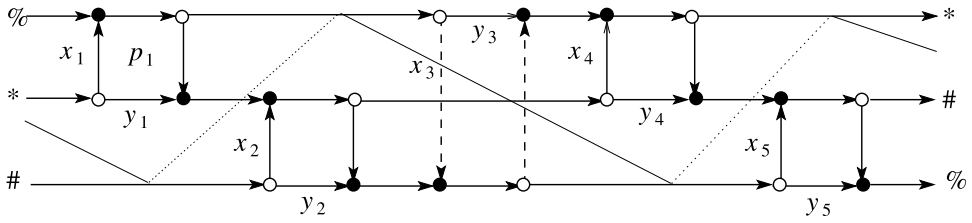

Fig. 7. The network $\bar{\mathcal{N}}_{3,5}$ on the torus.

The network $\bar{\mathcal{N}}_{3,5}$ is shown in Fig. 7. The figure depicts a torus, represented as a flattened two-sided cylinder (the dashed lines are on the "invisible" side); the edges marked by the same symbol are glued together accordingly. The cut is shown by the thin line. The meaning of the weights x_i and y_i will be explained later.

Proposition 3.1. *The directed dual of $\bar{\mathcal{N}}_{k,n}$ is isomorphic to $\mathcal{Q}_{k,n}$.*

Proof. It follows from the construction above that $\bar{\mathcal{N}}_{k,n}$ has $2n$ faces, n of them quadrilaterals and other n octagons. The quadrilateral faces correspond to p-vertices of the directed dual, and octagonal, to its q-vertices. Consider the quadrilateral corresponding to p_i. The four adjacent octagons are labeled as follows: the one to the left is q_{i-r-1}, the

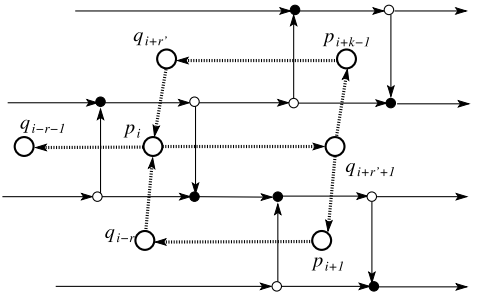

Fig. 8. The local structure of the directed dual of $\bar{\mathcal{N}}_{k,n}$.

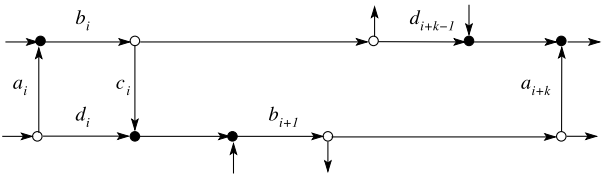

Fig. 9. Edge weights prior to the gauge group action.

one above is $q_{i+r'}$, the one to the right is $q_{i+r'+1}$, and the one below is q_{i-r}. Therefore, the octagonal face to the left of the quadrilateral p_{i+1} is q_{i-r}, and the one above it is $q_{i+r'+1}$, which justifies the first gluing rule above. Similarly, the octagonal face to the left of the quadrilateral p_{i+k-1} is $q_{i+k-2-r} = q_{i+r'}$, and the one below it is $q_{i+k-1-r} = q_{i+r'+1}$, which justifies the second gluing rule above, see Fig. 8, where the directed dual is shown with dotted lines. Therefore, we have restored the adjacency structure of $\mathcal{Q}_{k,n}$. □

Corollary 3.2. *The restriction of the standard Poisson bracket to the space of face weights of $\bar{\mathcal{N}}_{k,n}$ coincides with the bracket $\{\cdot,\cdot\}_k$.*

Proof. Follows immediately from (3.1) and Proposition 3.1, see Fig. 8. □

Assume that the edge weights around the face p_i are a_i, b_i, c_i, and d_i, and all other weights are equal 1, see Fig. 9. Besides, assume that

$$\prod_{i=1}^{n} b_i c_i = 1. \tag{3.4}$$

In what follows we will only deal with weights satisfying the above two conditions.

Applying the gauge group action, we can set to 1 the weights of the upper and the right edges of each quadrilateral face, while keeping weights of all edges with both endpoints of the same color equal to 1. For the face p_i, denote by x_i the weight of the left edge and by y_i, the weight of the lower edge after the gauge group action (see Fig. 7). Put $\mathbf{x} = (x_1, \dots, x_n)$, $\mathbf{y} = (y_1, \dots, y_n)$.

Proposition 3.3. (i) *The weights* $(\mathbf{x}, \mathbf{y})$ *are given by*

$$x_i = a_i b_{i-k+1} \prod_{j=i-k+1}^{i-1} b_j^{-1} c_j^{-1}, \qquad y_i = d_i b_{i-k+1} \prod_{j=i-k+1}^{i} b_j^{-1} c_j^{-1}. \tag{3.5}$$

(ii) *The relation between* $(\mathbf{p}, \mathbf{q})$ *and* $(\mathbf{x}, \mathbf{y})$ *is as follows:*

$$p_i = \frac{y_i}{x_i}, \quad q_i = \frac{x_{i+r+1}}{y_{i+r}}; \qquad x_i = x_1 \prod_{j=1}^{i-1} p_j q_{j-r}, \quad y_i = x_i p_i. \tag{3.6}$$

Proof. (i) Assume that the gauge group action is given by g_i^1 at the upper left vertex of the ith quadrilateral, by g_i^2 at the upper right vertex, by g_i^3 at the lower left vertex, and by g_i^4 at the lower right vertex. The conditions on the upper and right edges of the quadrilateral give $b_i g_i^1 / g_i^2 = 1$ and $c_i g_i^2 / g_i^4 = 1$, while the conditions on the two external edges going right from the quadrilateral give $g_i^4 = g_{i+1}^1$ and $g_i^2 = g_{i+k-1}^3$. Denote $\rho_i = g_i^1 / g_i^3$. From the first three equations above we get $g_{i+1}^3 = g_i^3 b_i c_i \rho_i / \rho_{i+1}$. Iterating this relation $i + k - 1$ times and taking into account the fourth equation above we arrive at $\rho_{i+k-1} = b_i^{-1} \prod_{j=i}^{i+k-2} b_j c_j$, or

$$\rho_i = b_{i-k+1}^{-1} \prod_{j=i-k+1}^{i-1} b_j c_j.$$

Now the first relation in (3.5) is restored from $x_i = a_i g_i^3 / g_i^1 = a_i / \rho_i$. To find y_i we write

$$y_i = d_i \frac{g_i^3}{g_i^4} = d_i \frac{g_i^3}{g_i^1} \frac{g_i^1}{g_i^2} \frac{g_i^2}{g_i^4} = \frac{d_i}{\rho_i b_i c_i},$$

which justifies the second relation in (3.5). Note that n-periodicity of ρ_i, and hence of x_i and y_i, is guaranteed by condition (3.4).

(ii) The expression for p_i follows immediately from the definition of face weights. Next, the face weight for the octagonal face to the right of p_i is $q_{i+r'+1} = x_{i+k} / y_{i+k-1}$, which yields $q_i = x_{i+k-r'-1} / x_{i+k-r'-2} = x_{i+r+1} / x_{i+r}$. The remaining two formulas in (3.6) are direct consequences of the first two. □

Note that by (3.6), the projection $\pi_k : (\mathbf{x}, \mathbf{y}) \mapsto (\mathbf{p}, \mathbf{q})$ has a one-dimensional fiber. Indeed, multiplying x and y by the same coefficient t does not change the corresponding p and q.

It follows immediately from (3.6) that $\prod_{i=1}^{n} p_i q_i = 1$, so the relevant map is $\overline{T}_k^{(1)}$. Let us show how it can be described via equivalent transformations of the network $\bar{\mathcal{N}}_{k,n}$. The transformations include Postnikov's moves of types 1, 2, and 3, and the gauge group action. We describe the sequence of these transformations below.

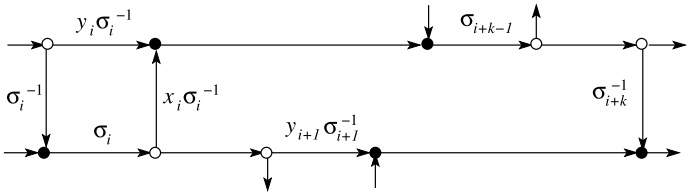

Fig. 10. Type 3 Postnikov's move for $\bar{\mathcal{N}}_{k,n}$.

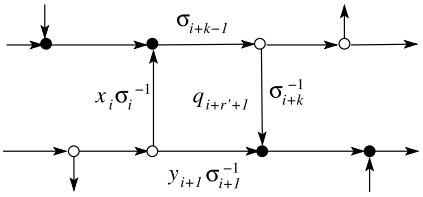

Fig. 11. Type 1 and 2 Postnikov's moves for $\bar{\mathcal{N}}_{k,n}$.

We start with the network $\bar{\mathcal{N}}_{k,n}$ with weights x_i and y_i on the left and lower edge of each quadrilateral face. First, we apply Postnikov's type 3 move at each p-face (this corresponds to cluster τ-transformations at p-vertices of $\mathcal{Q}_{k,n}$ given by (2.3)). To be able to use the type 3 move as shown in Fig. 4 we have first to conjugate it with the gauge action at the lower right vertex, so that $w_1 = x_i$, $w_2 = 1/y_i$, $w_3 = 1$, $w_4 = y$. Locally, the result is shown in Fig. 10 where $\sigma_i = x_i + y_i$.

Next, we apply type 1 and type 2 Postnikov's moves at each white–white and black–black edge, respectively. In particular, we move vertical arrows interchanging the right-most and the left-most position on the network in Fig. 7 using the fact that it is drawn on the torus. These moves interchange the quadrilateral and octagonal faces of the graph thereby swapping the variables p and q, see Fig. 11.

It remains to use gauge transformations to achieve the weights as in Fig. 7. In our situation, weights a_i, b_i, c_i, d_i are as follows, see Fig. 11:

$$a_i = \frac{x_i}{\sigma_i}, \quad b_i = \sigma_{i+k-1}, \quad c_i = \frac{1}{\sigma_{i+k}}, \quad d_i = \frac{y_{i+1}}{\sigma_{i+1}}. \tag{3.7}$$

Note that condition (3.4) is satisfied. This yields the map T_k, the main character of this paper, described in the following proposition.

Proposition 3.4. (i) *The map T_k is given by*

$$x_i^* = x_{i-r'-1}\frac{x_{i+r} + y_{i+r}}{x_{i-r'-1} + y_{i-r'-1}}, \quad y_i^* = y_{i-r'}\frac{x_{i+r+1} + y_{i+r+1}}{x_{i-r'} + y_{i-r'}}, \tag{3.8}$$

(ii) *The maps T_k and $\overline{T}_k^{(1)}$ are conjugated via π_k: $\pi_k \circ T_k = \overline{T}_k^{(1)} \circ \pi_k$.*

Proof. (i) Applying relations (3.5) to the weights (3.7) we get

$$x^*_{i+r'+1} = x_i \frac{\sigma_{i+k-1}}{\sigma_i}, \qquad y^*_{i+r'+1} = y_{i+1} \frac{\sigma_{i+k}}{\sigma_{i+1}},$$

which immediately implies (3.8).

(ii) Checked straightforwardly using (2.1), (3.6), and (3.8). □

Remark 3.5. Note that the map T_k commutes with the scaling action of the group $\mathbf{R}^*$: $(\mathbf{x}, \mathbf{y}) \mapsto (t\mathbf{x}, t\mathbf{y})$, and that the orbits of this action are the fibers of the projection π_k.

Maps T_2 and T_3 can be further described as follows. The map T_2 is a periodic version of the discretization of the relativistic Toda lattice suggested in [43]. It belongs to a family of Darboux–Bäcklund transformations of integrable lattices of Toda type, that were put into a cluster algebras framework in [14].

Proposition 3.6. *The map T_3 coincides with the pentagram map.*

Proof. Indeed, for $k = 3$, (3.8) gives

$$x^*_i = x_{i-2} \frac{x_i + y_i}{x_{i-2} + y_{i-2}}, \quad y^*_i = y_{i-1} \frac{x_{i+1} + y_{i+1}}{x_{i-1} + y_{i-1}}. \tag{3.9}$$

Change the variables as follows: $x_i \mapsto Y_i$, $y_i \mapsto -Y_i X_{i+1} Y_{i+1}$. In the new variables, the map (3.9) is rewritten as

$$X^*_i = X_{i-1} \frac{1 - X_{i-2}Y_{i-2}}{1 - X_i Y_i}, \quad Y^*_i = Y_i \frac{1 - X_{i+1}Y_{i+1}}{1 - X_{i-1}Y_{i-1}},$$

which becomes formula (1.1) after the cyclic shift $X_i \mapsto X_{i+1}$, $Y_i \mapsto Y_{i+1}$. Note that the maps T_k, and in particular the pentagram map, commute with this shift. □

Similarly to what was done in the previous section, we may consider, along with the map T_k based on p-dynamics $\overline{T}_k$, another map, based on q-dynamics $\overline{T}^\circ_k$; it is natural to denote this map by T°_k. Its definition differs from that of T_k by the order in which the same steps are performed. First of all, type 1 and 2 Postnikov's moves are applied, which leads to quadrilateral faces looking like those in Fig. 10. The weights of the left and the lower edge bounding the face labeled q_i are thus equal to 1, the weight of the upper edge equals y_{i+r}, and the weight of the right edge equals x_{i+r+1}. Next, the type 3 Postnikov's move is applied, followed by the gauge group action.

An alternative way to describe T°_k is to notice that the network $\bar{\mathcal{N}}_{k,n}$ can be redrawn in a different way. Recall that the network on the torus was obtained from the network on the cylinder by identifying the two boundary circles so that the cut ρ becomes a

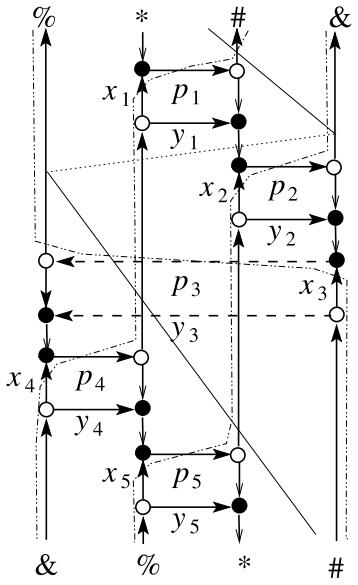

Fig. 12. An alternative representation of $\bar{\mathcal{N}}_{3,5}$.

closed curve. Conversely, the network on the cylinder is obtained from the network on the torus by cutting the torus along a closed curve. This curve intersects exactly once k monochrome edges: the black monochrome edge that points to the face p_1 and $k-1$ white monochrome edges that point to the faces $p_1, \dots, p_{k-1}$. Alternatively, the torus can be cut along a different closed curve that intersects the same black monochrome edge and all the $n-k+1$ remaining white monochrome edges. An alternative representation of $\bar{\mathcal{N}}_{3,5}$ is shown in Fig. 12. The cut shown in Fig. 12 coincides with that in Fig. 7. We can further reverse the closed path shown with the dashed line and apply type 1 and 2 Postnikov moves at all white–white and black–black edges. It is easy to see that the resulting network is isomorphic to $\bar{\mathcal{N}}_{4,5}$. In general, starting with $\bar{\mathcal{N}}_{k,n}$ and applying the same transformations one gets a network isomorphic to $\bar{\mathcal{N}}_{n-k+2,n}$, which hints that T_k° and T_{n-k+2} are related.

Introduce an auxiliary map D_k given by

$$x_i^* = \frac{1}{y_{i+r}} \prod_{j=i-r'}^{i+r} \frac{y_j}{x_j}, \qquad y_i^* = \frac{1}{y_{i+r+1}} \prod_{j=i-r'}^{i+r+1} \frac{y_j}{x_j}. \tag{3.10}$$

The following analog of Proposition 2.2 explains the relation between T, T^{-1} and T°.

Proposition 3.7. (i) *The maps T_k^{-1} and T_k° coincide and are given by*

$$x_i^* = x_{i+r'+1} \frac{x_{i-r} + y_{i-r-1}}{x_{i+r'+1} + y_{i+r'}}, \qquad y_i^* = y_{i+r'} \frac{x_{i-r} + y_{i-r-1}}{x_{i+r'+1} + y_{i+r'}}. \tag{3.11}$$

(ii) *The maps* T_k *and* T_k° *are almost conjugated by* D_k*:*

$$S_{r-r'} \circ T_k^\circ \circ D_k = D_k \circ T_k. \tag{3.12}$$

(iii) *Let* $D_{k,n}$ *be given by* $\bar{x}_i = y_{i-r-1}$, $\bar{y}_i = x_{i-r}$. *Then*

$$T_k^\circ = D_{k,n} \circ T_{n-k+2} \circ D_{n-k+2,n}.$$

Proof. (i) The proof of (3.11) for T_k^{-1} is similar to that of Proposition 2.2(i). It is easy to check that the maps D_k and $\overline{D}_k$ given by (3.10) and (2.4) are conjugated via π_k: $\pi_k \circ D_k = \overline{D}_k \circ \pi_k$. Besides, define the map C_k by

$$x_i^* = \frac{x_{i-k+1} + y_{i-k+1}}{y_{i-k+1}(x_i + y_i)} \prod_{j=i-k+1}^{i-1} \frac{y_j}{x_j}, \qquad y_i^* = \frac{x_{i-k+1} + y_{i-k+1}}{y_{i-k+1}(x_i + y_i)} \prod_{j=i-k+1}^{i} \frac{y_j}{x_j}.$$

Similarly, $\pi_k \circ C_k = \overline{C}_k \circ \pi_k$. Moreover, $T_k = C_k \circ D_k$. Therefore, $T_k^{-1} = D_k^{-1} \circ C_k^{-1}$.

A direct computation shows that C_k is an involution, while D_k^{-1} is given by

$$x_i^* = \frac{1}{y_{i+r'}} \prod_{j=i-r}^{i+r'} \frac{y_j}{x_j}, \qquad y_i^* = \frac{1}{y_{i+r'+1}} \prod_{j=i-r}^{i+r'+1} \frac{y_j}{x_j},$$

and (3.11) for T_k^{-1} follows.

To prove (3.11) for T_k° one has to perform all the steps described above, similarly to what was done in the proofs of Propositions 3.3 and 3.4.

(ii) Follows immediately from (i) and the relation $D_k^2 = S_{r-r'}$.

(iii) Checked straightforwardly taking into account (2.7). Note that transformations $D_{k,n}$ and $D_{n-k+2,n}$ are related to $\overline{D}_{k,n}$ via $\pi_{n-k+2} \circ D_{n-k+2,n} = \overline{D}_{k,n} \circ \pi_k$ and $\pi_k \circ D_{k,n} = \overline{D}_{k,n} \circ \pi_{n-k+2}$. □

4. Poisson structure and complete integrability

The main result of this paper is *complete integrability* of transformations T_k, i.e., the existence of a T_k-invariant Poisson bracket and of a maximal family of integrals in involution. The key ingredient of the proof is the result obtained in [15] on Poisson properties of the boundary measurement map defined in Section 3.1. First, we recall the definition of an R-matrix (Sklyanin) bracket, which plays a crucial role in the modern theory of integrable systems [30,8]. The bracket is defined on the space of $n \times n$ rational matrix functions $M(\lambda) = (m_{ij}(\lambda))_{i,j=1}^n$ and is given by the formula

$$\left\{ M(\lambda) \overset{\otimes}{,} M(\mu) \right\} = [R(\lambda, \mu), M(\lambda) \otimes M(\mu)], \tag{4.1}$$

where the left-hand side is understood as $\left\{M(\lambda)\overset{\otimes}{,}M(\mu)\right\}_{ii'}^{jj'} = \{m_{ij}(\lambda), m_{i'j'}(\mu)\}$ and an R-matrix $R(\lambda,\mu)$ is an operator in $(\mathbf{R}^n)^{\otimes 2}$ depending on parameters λ, μ and solving the classical Yang–Baxter equation. We are interested in the bracket associated with the *trigonometric R-matrix* (for the explicit formula for it, which we will not need, see [30]).

4.1. Cuts, rims, and conjugate networks

Let $\mathcal{N}$ be a perfect network on the cylinder; recall that $\bar{\mathcal{N}}$ stands for the perfect network on the torus obtained from $\mathcal{N}$ via the gluing procedure described in Section 3.1.

Theorem 4.1. *For any perfect network $\widehat{\mathcal{N}}$ on the torus, there exists a perfect network $\mathcal{N}$ on the cylinder with sources and sinks belonging to different components of the boundary such that $\bar{\mathcal{N}}$ is equivalent to $\widehat{\mathcal{N}}$, the map $\mathcal{E}_{\mathcal{N}} \to \mathcal{F}_{\widehat{\mathcal{N}}}$ is Poisson with respect to the standard Poisson structures, and spectral invariants of the image $M_{\mathcal{N}}(\lambda)$ of the boundary measurement map depend only on $\mathcal{F}_{\widehat{\mathcal{N}}}$. In particular, spectral invariants of $M_{\mathcal{N}}(\lambda)$ form an involutive family of functions on $\mathcal{F}_{\widehat{\mathcal{N}}}$ with respect to the standard Poisson structure.*

Proof. Consider a closed simple noncontractible oriented loop γ on the torus; we call it a *rim* if it does not pass through vertices of $\widehat{\mathcal{N}}$ and its intersection index with the cut ρ equals ± 1. To avoid unnecessary technicalities, we assume that γ and all edges of $\widehat{\mathcal{N}}$ are smooth curves. Besides, we assume that each edge intersects γ in a finite number of points and that all the intersections are transversal. Each intersection point defines an orientation of the torus via taking the tangent vectors to the edge and to the rim at this point and demanding that they form a right basis of the tangent plane. We say that the rim is *ideal* if its intersection points with all edges define the same orientation of the torus.

Proposition 4.2. *Let $\widehat{\mathcal{N}}$ be a perfect network on the torus, then there exists a rim which becomes ideal after a finite number of path reversals in $\widehat{\mathcal{N}}$.*

Proof. Consider the universal covering π of the torus by a plane. Take an arbitrary rim γ. The preimage $\pi^{-1}(\gamma)$ is a disjoint union of simple curves in the plane, each one isotopic to a line. Fix arbitrarily one such curve l_0; it divides the plane into two regions L and R lying to the left and to the right of the curve, respectively. Let l_i, $i \in \mathbf{N}$, be the connected components of $\pi^{-1}(\gamma)$ lying in R: l_1 is the first one to the right of l_0, l_2 is the next one, etc.

Let $\widehat{\mathcal{N}}_R$ be the part of the network covering $\widehat{\mathcal{N}}$ that belongs to R. Each intersection point of an edge of $\widehat{\mathcal{N}}$ with γ gives rise to a countable number of boundary vertices of $\widehat{\mathcal{N}}_R$ lying on l_0. Denote by m the number of intersection points of γ with the edges of $\widehat{\mathcal{N}}$. We will need the following auxiliary statement.

Lemma 4.3. *Let P be a possibly infinite oriented simple path in $\widehat{\mathcal{N}}_R$ that ends at a boundary vertex and intersects l_{m+1}. Then there exist i, j such that $m+1 \geq i > j \geq 0$ and points $t_i \in l_i$ and $t_j \in l_j$ on P such that t_i precedes t_j on P and $\pi(t_i) = \pi(t_j)$.*

Proof. Let us traverse P backwards starting from its endpoint, and let t_{m+1} be the first point on l_{m+1} that is encountered during this process. Further, let t_i for $0 \leq i \leq m$ be the first point on l_i that is encountered while traversing P forward from t_{m+1}; in particular, t_0 is the endpoint of P. The proof now follows from the pigeonhole principle applied to the nested intervals of P between the points t_{m+1} and t_i. □

Assume that $\widehat{\mathcal{N}}_R$ contains a path P as in Lemma 4.3. Consider the interval P_{ij} of P between the points t_i and t_j described in the lemma. Clearly $\pi(P_{ij})$ is a closed non-contractible path on the torus. If $\pi(P_{ij})$ is a simple path, its reversal increases by one the number of intersection points on γ that define a right basis. If $\pi(P_{ij})$ is not simple and s is a point of selfintersection, it can be decomposed into a path from $\pi(t_i)$ to s, a loop through s, and a path from s to $\pi(t_j)$. Further, the loop can be erased, and the remaining two parts glued together, which results in a closed path on the torus with a smaller number of selfintersection points. After a finite number of such steps we arrive at a simple closed path on the torus that can be reversed.

Proceeding in this way, we get a network $\widehat{\mathcal{N}}'$ on the torus equivalent to $\widehat{\mathcal{N}}$ such that any path in $\widehat{\mathcal{N}}'_R$ that ends at a boundary vertex does not intersect l_{m+1}. Note that a path like that may still be infinite. Each such path divides R into two regions: one of them contains l_{m+1}, while the other one is disjoint from it. Let A be the intersection of the regions containing l_{m+1} over all paths P in $\widehat{\mathcal{N}}'_R$, and let ∂A be its boundary. Clearly, ∂A is invariant under the translations that commute with π and take each l_i into itself. Therefore, $\pi(\partial A)$ is a simple loop on the torus, and it is homologous to γ; it is not a rim yet since it contains edges and vertices of $\widehat{\mathcal{N}}'$.

Each vertex v lying on $\pi(\partial A)$ has three incident edges. Two of them lie on $\pi(\partial A)$ as well. Since a preimage t of v belongs to ∂A, the preimages of these two edges incident to t belong to paths that end at l_0. Therefore, if the third edge incident to v is pointed towards v, its preimage incident to t should belong to the complement of A, by the definition of A.

Now, to build a rim, we take a tubular ε-neighborhood of ∂A, and consider the boundary $\partial A_{+\varepsilon}$ of this tubular neighborhood that lies inside A. For ε small enough, the above property of the vertices lying on $\pi(\partial A)$ guarantees that the rim $\pi(\partial A_{+\varepsilon})$ intersects only those edges that point from these vertices into A, and hence each intersection point defines a right basis. Therefore $\pi(\partial A_{+\varepsilon})$ is an ideal rim. □

Returning to the proof of the theorem, we apply Proposition 4.2 to find the corresponding ideal rim on the torus. Let $\mathcal{N}$ be the network obtained from $\widehat{\mathcal{N}}'$ after we cut the torus along this rim. Note that each edge of $\widehat{\mathcal{N}}'$ that intersects the rim yields several (two or more) edges in $\mathcal{N}$; the weights of these edges are chosen arbitrarily subject to the

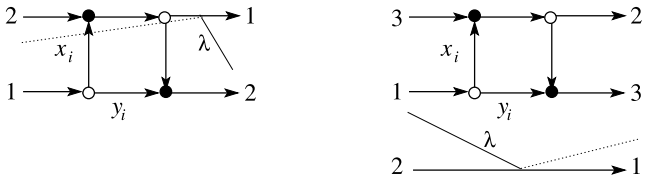

Fig. 13. Elementary networks.

condition that their product equals the weight of the initial edge. By Proposition 4.2, all sources of $\widehat{\mathcal{N}}'$ belong to one of its boundary circles, while all sinks belong to the other boundary circle. Besides, $\bar{\mathcal{N}} = \widehat{\mathcal{N}}'$, and hence $\widehat{\mathcal{N}}$ and $\bar{\mathcal{N}}$ are equivalent. Clearly, one can choose a new cut ρ' on the torus isotopic to ρ such that it intersects the rim only once. Consequently, after the torus is cut into a cylinder, ρ' becomes a cut on the cylinder.

The rest of the proof relies on two facts. One is Theorem 3.13 of [15]: *for any network on a cylinder with the equal number of sources and sinks belonging to different components of the boundary, the standard Poisson structure on the space of edge weights induces the trigonometric R-matrix bracket on the space of boundary measurement matrices.* The second is a well-known statement in the theory of integrable systems: *spectral invariants of $M_{\mathcal{N}}(\lambda)$ are in involution with respect to the Sklyanin bracket*, see Theorem 12.24 in [30]. □

We can now apply Theorem 4.1 to the network $\bar{\mathcal{N}}_{k,n}$. Clearly, one can choose the rim γ in such a way that the resulting network on a cylinder will be $\mathcal{N}_{k,n}$. Note that in this case no path reversals are needed. For example, for the network $\bar{\mathcal{N}}_{3,5}$, γ can be represented by a closed curve slightly to the left of the edge marked x_1 and transversal to all horizontal edges. The resulting network $\mathcal{N}_{3,5}$ can be seen in Fig. 7, provided we refrain from gluing together edges marked with the same symbols and regard that figure as representing a cylinder rather than a torus. Furthermore, this network on a cylinder is a concatenation of n *elementary networks* of the same form shown on Fig. 13 (for the cases $k = 2$ and $k = 3$).

Since elementary networks are acyclic, the corresponding boundary measurement matrices are

$$L_i(\lambda) = \begin{pmatrix} -\lambda x_i & x_i + y_i \\ -\lambda & 1 \end{pmatrix}$$

for $k = 2$ and

$$L_i(\lambda) = \begin{pmatrix} 0 & 0 & 0 & \dots & x_i & x_i + y_i \\ -\lambda & 0 & 0 & \dots & 0 & 0 \\ 0 & 1 & 0 & \dots & 0 & 0 \\ 0 & 0 & 1 & \dots & 0 & 0 \\ \dots & \dots & \dots & \dots & \dots & \dots \\ 0 & 0 & 0 & \dots & 1 & 1 \end{pmatrix} \tag{4.2}$$

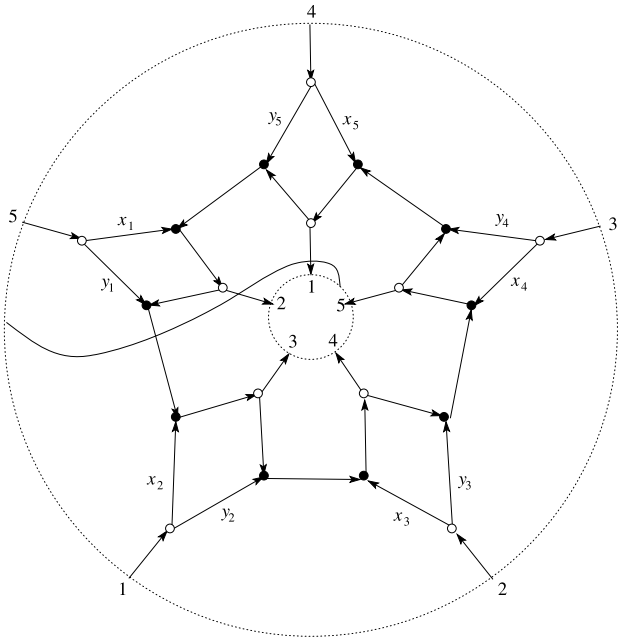

Fig. 14. The conjugate network $\mathcal{N}'_{3,5}$.

for $k \geq 3$ (negative signs are implied by the sign conventions mentioned in Section 3.1). Consequently, the boundary measurement matrix that corresponds to $\mathcal{N}_{k,n}$ is

$$M_{k,n}(\lambda) = L_1(\lambda) \cdots L_n(\lambda). \tag{4.3}$$

In our construction above, the cut ρ and the rim γ are represented by non-contractible closed curves from two distinct homology classes; to get the network $\mathcal{N}_{k,n}$ on the cylinder we start from the network $\bar{\mathcal{N}}_{k,n}$ on the torus and cut it along γ so that ρ becomes a cut in $\mathcal{N}_{k,n}$. One can interchange the roles of ρ and γ and to cut the torus along ρ, making γ a cut. This gives another perfect network $\mathcal{N}'_{k,n}$ on the cylinder with n sources and n sinks belonging to different components of the boundary. To this end, we first observe that ρ intersects all $\circ \to \circ$ edges and no other edges of $\bar{\mathcal{N}}_{k,n}$ (see Fig. 13). We label the resulting intersection points along ρ by numbers from 1 to n in such a way that the point seen on Fig. 13 is labeled by i (for $k \geq 3$ this point belongs to the edge that connects the source 2 with the sink 1). Next, we cut the torus along ρ. Each of the newly labeled intersection points gives rise to one source and one sink in $\mathcal{N}'_{k,n}$. The rim γ becomes the cut ρ' for $\mathcal{N}'_{k,n}$. It is convenient to view $\mathcal{N}'_{k,n}$ as a network in an annulus with sources on the outer boundary circle and sinks on the inner boundary circle. The cut ρ' starts at the segment between sinks n and 1 on the inner circle and ends on the corresponding segment on the outer circle. It is convenient to assume that in between it crosses $k-1$ edges incident to the inner boundary, followed by a single $\bullet \to \bullet$ edge (see Fig. 14). The

variable associated with the cut in $\mathcal{N}'_{k,n}$ will be denoted by z. We will say that $\mathcal{N}'_{k,n}$ is *conjugate* to $\mathcal{N}_{k,n}$.

Proposition 4.4. *Let* $D_x = \operatorname{diag}(x_1, \dots, x_n)$, $D_y = \operatorname{diag}(y_1, \dots, y_n)$, *and* $Z = -ze_{n1} + \sum_{i=1}^{n-1} e_{i,i+1}$. *The boundary measurement matrix* $A_{k,n}(z) = (a_{ij}(z))_{i,j=1}^{n}$ *for the network* $\mathcal{N}'_{k,n}$ *is given by*

$$A_{k,n}(z) = Z\,(D_x + D_y Z)\,Z^{k-2}\,(\mathbf{1}_n - Z)^{-1}\,. \tag{4.4}$$

Proof. For any source i and sink j there are exactly two simple (non-self-intersecting) directed paths in $\mathcal{N}'_{k,n}$ directed from i to j: one contains the edge of weight x_{i+1}, and the other, the edge of weight y_{i+1}. Every such path has a subpath in common with the unique oriented cycle in $\mathcal{N}'_{k,n}$ that contains all edges of weight 1 that are not incident to either of the boundary components. The weight of this cycle is z, which means that all boundary measurements $a_{ij}(z)$ acquire a common factor $1 - z + z^2 - \ldots = \frac{1}{1+z}$ (see the sign conventions in Section 3.1). The simple directed path from i to j containing the edge of weight x_{i+1} intersects the cut once if $k - n - 1 \le j - i < k - 1$, twice if $j - i < k - n - 1$, and does not intersect the cut if $j - i \ge k - 1$. The simple directed path from i to j containing the edge of weight y_{i+1} intersects the cut once if $k - n \le j - i < k$, twice if $j - i < k - n$, and does not intersect the cut if $j - i \ge k$. All intersections are positive. Thus, by the sign conventions,

$$(1+z)a_{ij}(z) = \begin{cases} x_{i+1} + y_{i+1} & \text{if } j - i > k - 1, \\ x_{i+1} - zy_{i+1} & \text{if } j - i = k - 1, \\ -z(x_{i+1} + y_{i+1}) & \text{if } k - n - 1 < j - i < k - 1, \\ -z(x_{i+1} - zy_{i+1}) & \text{if } j - i = k - n - 1, \\ z^2(x_{i+1} + y_{i+1}) & \text{if } j - i < k - n - 1. \end{cases}$$

or, equivalently,

$$A_{k,n}(z) = \frac{1}{1+z} \times \left(\operatorname{diag}(x_2, \dots, x_n, x_1) + \operatorname{diag}(y_2, \dots, y_n, y_1)Z\right)\left(Z^{k-1} + \ldots + Z^{n+k-2}\right).$$

Here we used the relation $Z^n = -z\mathbf{1}_n$. The claim now follows from the identities

$$Z \operatorname{diag}(d_1, \dots, d_n) Z^{-1} = \operatorname{diag}(d_2, \dots, d_n, d_1) \tag{4.5}$$

and

$$(\mathbf{1}_n - Z)^{-1} = \frac{1}{1+z}\left(\mathbf{1}_n + \ldots + Z^{n-1}\right). \qquad \square \tag{4.6}$$

4.2. Poisson structure

Let $\mathcal{M}_{k,n}$ and $\mathcal{A}_{k,n}$ be images of the boundary measurement maps from $\mathcal{E}_{\mathcal{N}_{k,n}}$ and $\mathcal{E}_{\mathcal{N}'_{k,n}}$ respectively. Theorem 4.1 implies that spectral invariants of elements of $\mathcal{M}_{k,n}$ and $\mathcal{A}_{k,n}$ viewed as functions on $\mathcal{F}_{\bar{\mathcal{N}}_{k,n}}$ are in involution with respect to the standard Poisson structure. However, quantities x_n, y_n, and therefore the spectral invariants of $M_{k,n}(\lambda)$ and $A_{k,n}(z)$ are only defined as functions on a subset $\mathcal{F}^1_{\bar{\mathcal{N}}_{k,n}}$ specified by the condition (3.4).

Proposition 4.5. (i) *$\mathcal{F}^1_{\bar{\mathcal{N}}_{k,n}}$ is a Poisson submanifold of $\mathcal{F}_{\bar{\mathcal{N}}_{k,n}}$ with respect to the standard Poisson structure. For $n \geq 2k-1$, the restriction of the standard Poisson structure to $\mathcal{F}^1_{\bar{\mathcal{N}}_{k,n}}$ is given by*

$$\begin{aligned} &\{x_i, x_{i+l}\} = -x_i x_{i+l},\ 1 \leq l \leq k-2; \quad \{y_i, y_{i+l}\} = -y_i y_{i+l},\ 1 \leq l \leq k-1; \\ &\{y_i, x_{i+l}\} = -y_i x_{i+l},\ 1 \leq l \leq k-1; \quad \{y_i, x_{i-l}\} = y_i x_{i-l},\ 0 \leq l \leq k-2, \end{aligned} \tag{4.7}$$

where indices are understood mod n *and only non-zero brackets are listed.*

(ii) *The bracket (4.7) has rank $2(n-d)$, where $d = \gcd(k-1, n)$. Functions*

$$\prod_{i=0}^{\frac{n}{d}-1} x_{s+i(k-1)}, \qquad \prod_{i=0}^{\frac{n}{d}-1} y_{s+i(k-1)}, \quad s = 1, \dots, d, \tag{4.8}$$

are Casimir functions for (4.7).

(iii) *The bracket (4.7) is invariant under the map T_k.*

Proof. (i) As was explained in Section 3.1, $\mathcal{F}_{\bar{\mathcal{N}}_{k,n}}$ can be parameterized by face coordinates p_i, q_i, $i = 1, \dots, n$, subject to $\prod_{i=1}^n p_i q_i = 1$ and weights z, z_ρ of two trails that we will choose as follows. The trail that corresponds to z_ρ is a directed cycle P_ρ that traces the $\bullet \to \circ \to \bullet$ part of the boundary of each quadrilateral face p_i and the immediately following $\bullet \to \bullet$ edge of the corresponding octagonal face $q_{i+r'+1}$, see Fig. 8. After applying the gauge action to ensure that weights of all monochrome edges are equal to 1, we see that the weight z_ρ is equal to $\prod_{i=1}^n b_i c_i$, where we are using notations from Section 3.2. The weight z corresponds to the directed cycle P that consists of the $\circ \to \circ$ edge separating octagonal faces q_{n-r} and q_{n+1-r} followed by the $\circ \to \bullet$ edge of the quadrilateral p_1 followed by the subpath of P_ρ that closes the cycle. (For example, for $\bar{\mathcal{N}}_{3,5}$ depicted in Fig. 7, P_ρ contains the $\circ \to * \to \circ$ edge followed by the $\circ \to \bullet$ edge labeled by x_1.) Since $\mathcal{F}^1_{\bar{\mathcal{N}}_{k,n}}$ is cut out from $\mathcal{F}_{\bar{\mathcal{N}}_{k,n}}$ by condition (3.4) (or, equivalently, $z_\rho = 1$), to see that $\mathcal{F}^1_{\bar{\mathcal{N}}_{k,n}}$ is a Poisson submanifold of $\mathcal{F}_{\bar{\mathcal{N}}_{k,n}}$, we need to check that Poisson brackets of z_ρ with z and all face weights with respect to the standard Poisson structure are zero. For the bracket $\{z_\rho, z\}$ this claim follows from (3.3): there is only

one maximal common subpath of P and P_ρ, and the relative position of the paths is as on Fig. 5a). For the bracket $\{z_\rho, y_f\}$ the claim follows from (3.2). If f is a quadrilateral face then there is only one path P' in the outer sum; it consists of two edges, and the corresponding edges of the directed dual are opposite, see Fig. 8. If f is an octagonal face then there are two paths P' in the outer sum. One of them consists of three edges, of which one is monochrome; the edges of the directed dual corresponding to the remaining two edges of P' are opposite, see Fig. 8. The second one consists of a unique monochrome edge.

Next, $\mathcal{F}^1_{\bar{\mathcal{N}}_{k,n}}$ can be parameterized by either x_i, y_i, $i = 1, \dots, n$, or by p_i, q_i, $i = 1, \dots, n$, $\prod_{i=1}^n p_i q_i = 1$, and z. To finish the proof of statement (i), it suffices to show that brackets (4.7) generate the same Poisson relations among p_i, q_i, z as the standard Poisson structure on $\mathcal{F}_{\bar{\mathcal{N}}_{k,n}}$. Recall that by Corollary 3.2, the Poisson brackets between p_i, q_i in the standard Poisson structure coincide with those given by $\{\cdot,\cdot\}_k$. Furthermore, it follows from (3.2) that $\{z, q_i\} = 0$ and $\{z, p_j\} = (\delta_{1,j} - \delta_{n-k+2,j})\, z p_j$. Note that due to (3.4) and gauge-invariance of weights of directed cycles, $z = x_1$ on $\mathcal{F}^1_{\bar{\mathcal{N}}_{k,n}}$. This, together with the periodicity of $\bar{\mathcal{N}}_{k,n}$, leads to Poisson brackets $\{x_i, p_j\} = (\delta_{i,j} - \delta_{i-k+1,j})\, x_i p_j$.

For an n-tuple $(u_1, \dots, u_n)$, let $\bar{\mathbf{u}}$ be the column vector $(\log u_i)_{i=1}^n$. For two n-tuples $(u_1, \dots, u_n)$, $(v_1, \dots, v_n)$ of functions on a Poisson manifold, we use a shorthand notation $\{\bar{\mathbf{u}}, \bar{\mathbf{v}}^T\}$ to denote a matrix of Poisson brackets $(\{\log u_i, \log v_j\})_{i,j=1}^n$. Note that $\{\bar{\mathbf{v}}, \bar{\mathbf{u}}^T\} = -\{\bar{\mathbf{u}}, \bar{\mathbf{v}}^T\}^T$.

We can then describe the Poisson brackets $\{p_i, q_j\}$, $\{p_i, p_j\}$, $\{q_i, q_j\}$, $\{x_i, p_j\}$ by

$$\begin{aligned} \{\bar{\mathbf{p}}, \bar{\mathbf{q}}^T\} &= C^{-r-1} + C^{r'+1} - C^{-r} - C^{r'}, \\ \{\bar{\mathbf{p}}, \bar{\mathbf{p}}^T\} = \{\bar{\mathbf{q}}, \bar{\mathbf{q}}^T\} = \{\bar{\mathbf{x}}, \bar{\mathbf{q}}^T\} &= 0, \quad \{\bar{\mathbf{x}}, \bar{\mathbf{p}}^T\} = \mathbf{1} - C^{1-k}, \end{aligned} \tag{4.9}$$

where $C = e_{12} + \cdots + e_{n-1n} + e_{n1} = S + e_{n1}$ is an $n \times n$ cyclic shift matrix and S is an upper triangular shift matrix. Similarly, formulas in (4.7) are equivalent, provided $n \geq 2k - 1$, to

$$\begin{aligned} \Omega_x := \{\bar{\mathbf{x}}, \bar{\mathbf{x}}^T\} &= \sum_{i=1}^{k-2} \left(C^{-i} - C^i\right) = (\mathbf{1} - C^{k-1}) \sum_{i=1}^{k-2} C^{-i}, \\ \Omega_y := \{\bar{\mathbf{y}}, \bar{\mathbf{y}}^T\} &= \sum_{i=1}^{k-1} \left(C^{-i} - C^i\right) = (\mathbf{1} - C^{k-1}) \sum_{i=0}^{k-1} C^{-i}, \\ \Omega_{yx} := \{\bar{\mathbf{y}}, \bar{\mathbf{x}}^T\} &= \sum_{i=1}^{k-1} \left(C^{1-i} - C^i\right) = (\mathbf{1} - C^{k-1}) \sum_{i=0}^{k-2} C^{-i}. \end{aligned} \tag{4.10}$$

We need to check that relations (4.10) imply (4.9). This follows via a straightforward calculation from relations $\bar{\mathbf{p}} = \bar{\mathbf{y}} - \bar{\mathbf{x}}$, $\bar{\mathbf{q}} = C^r\,(C\bar{\mathbf{x}} - \bar{\mathbf{y}})$ induced by (3.6) (one also needs to take into account equalities $r + r' = k - 2$ and $C^T = C^{-1}$).

(ii) The rank of the Poisson bracket (4.7) is equal to the rank of the matrix

$$\Omega = \begin{pmatrix} \Omega_x & -\Omega_{yx}^T \\ \Omega_{yx} & \Omega_y \end{pmatrix}.$$

The claim that functions (4.8) are Casimir functions follows from (4.10) and the fact that vectors $\sum_{i=0}^{\frac{n}{d}-1} e_{s+i(k-1)}$, $s = 1, \dots, d$, form a basis of the kernel of $\mathbf{1} - C^{k-1}$. Let V be the complement to that kernel in $\mathbf{R}^n$ spanned by vectors $(v_i)_{i=1}^n$ such that $\sum_{i=0}^{\frac{n}{d}-1} v_{s+i(k-1)} = 0$ for $s = 1, \dots, d$. Then V is invariant under C, $\mathbf{1} - C^{k-1}$ is invertible on V and the rank of Ω is equal to the rank of its restriction to $V \oplus V$. On $V \oplus V$, we define

$$A = \begin{pmatrix} C(C-\mathbf{1})^{-1} & -(C-\mathbf{1})^{-1} \\ -\mathbf{1} & \mathbf{1} \end{pmatrix}$$

and compute

$$A\Omega A^T = \begin{pmatrix} 0 & C^{1-k} - \mathbf{1} \\ \mathbf{1} - C^{k-1} & 0 \end{pmatrix}.$$

Since $A\Omega A^T$ is invertible on $V \oplus V$, we conclude that the rank of (4.7) is $2(n-d)$.

(iii) Invariance of (4.7) under the map T_k can be verified by a direct calculation. □

Remark 4.6. There are formulae similar to (4.7) for T_k-invariant Poisson bracket in the case $n < 2k-1$ as well. Our focus on the "stable range" $n \geq 2k-1$ will be justified by the geometric interpretation of the maps T_k in Section 5.

4.3. Conserved quantities

The ring of spectral invariants of $M_{k,n}(\lambda)$ is generated by coefficients of its characteristic polynomial

$$\det(I_n + zM_{k,n}(\lambda)) = \sum_{i=1}^{n} \sum_{j=1}^{k} I_{ij}(x,y)\lambda^i z^j. \tag{4.11}$$

(Some of the coefficients I_{ij} are identically zero.)

Proposition 4.7. *Functions $I_{ij}(x,y)$ are invariant under the map T_k.*

Proof. Recall that in Section 3.2, T_k was described via a sequence of Postnikov's moves and gauge transformations. Furthermore, $\mathcal{N}_{k,n}$ is obtained from $\bar{\mathcal{N}}_{k,n}$ by cutting the torus into a cylinder along an ideal rim γ. Note that type 3 Postnikov's moves and

gauge transformations do not affect the boundary measurement matrix. In fact, the only transformations that do change the boundary measurements are type 1 and 2 moves interchanging vertical edges lying on different sides of γ. For a network on a cylinder, moving a vertical edge past γ from left to right is equivalent to cutting at the right end of the cylinder a thin cylindrical slice containing this edge and no other vertical edges and then reattaching this slice to the cylinder on the left. In terms of boundary measurement matrices, this operation amounts to a matrix transformation of the form $M = AB \mapsto \tilde{M} = BA$ under which non-zero eigenvalues of M and $\tilde{M}$ coincide. This proves the claim. □

Next, we will provide a combinatorial interpretation of conserved quantities I_{ij} in terms of the network $\bar{\mathcal{N}}_{k,n}$. This, in turn, will allow us to clarify the relation between boundary measurements $M_{k,n}(\lambda)$ and $A_{k,n}(z)$ in the context of the map T_k.

Let $\mathcal{N}$ be a perfect network on the torus with the cut ρ, and let γ be a rim. For an arbitrary simple directed cycle C in $\mathcal{N}$ we define its weight $w(C)$ as the product of the weights of the edges in C times $(-1)^{d_\lambda+d_z}\lambda^{d_\lambda}z^{d_z}$, where d_λ and d_z are the intersection indices of C with ρ and γ, respectively. The weight of a collection $\mathcal{C}$ of disjoint simple cycles is defined as $w(\mathcal{C}) = (-1)^{|\mathcal{C}|}\prod_{C\in\mathcal{C}} w(C)$. Finally, define the function $\mathfrak{P}_{\mathcal{N}}(\lambda, z) = \sum w(\mathcal{C})$, where the sum is taken over all collections of disjoint simple cycles.

Proposition 4.8. *Let $\mathcal{N}$ be a perfect network on the torus with no contractible cycles, γ be an ideal rim, and $M(\lambda)$ be the $m \times m$ boundary measurement matrix for the network on the cylinder obtained by cutting the torus along γ. Then*

$$\det(I_m + zM(\lambda)) = \frac{\mathfrak{P}_{\mathcal{N}}(\lambda, z)}{\mathfrak{P}_{\mathcal{N}}(\lambda, 0)}. \tag{4.12}$$

Proof. First of all, note that

$$\det(I_m + zM(\lambda)) = 1 + \sum_{j=1}^{m} z^j \sum_{|J|=j} \Delta^J(M(\lambda)), \tag{4.13}$$

where $\Delta^J(M(\lambda))$ is the principal $j \times j$ minor of $M(\lambda)$ with the row and column sets J. To evaluate this minor we use the formula for determinants of weighted path matrices obtained in [45].

It is important to note that there are two distinctions between the definitions of the path weights here and in [45]. First, there is no cut in [45]. This can be overcome by modifying edge weights: if an edge of weight w intersects the cut, then its weight is changed to λw or $\lambda^{-1}w$, depending on the orientation of the intersection; see Chapter 9.1.1 in [13] for details. Second, the sign conventions in [45] are different from those described in Section 3.1: the sign of any path is positive. However, in the absence of contractible cycles our conventions can emulate conventions of [45]. To achieve that, it suffices to apply the transformation $\lambda \mapsto -\lambda$. Indeed, after the torus is cut along γ, the only cycles in $\mathcal{N}$

that survive are those with $d_\lambda = \pm 1$. By our sign conventions, such cycles contribute -1 to the sign of a path. The same result is achieved if the contribution to the sign of a path is 1, and the weight of the appropriate edge is multiplied (or divided) by $-\lambda$. Paths on the cylinder that intersect the cut ρ are treated in a similar way. Finally, the rim γ is ideal, and hence the sources and the sinks lie on different boundary circles of the cylinder. Therefore,

$$\Delta^J(M(\lambda)) = \Delta^{J,m+J}(\bar{W}(-\lambda)), \tag{4.14}$$

where $\bar{W}(-\lambda)$ is the path weight matrix built by the rules of [45] based on modified weights of the edges.

It follows from the main theorem of [45] that

$$\Delta^{J,m+J}(\bar{W}) = \frac{\sum_{\mathcal{D}} \operatorname{sgn}(\mathcal{D})\bar{w}(\mathcal{D})}{\sum_{\mathcal{C}}(-1)^{|\mathcal{C}|}\bar{w}(\mathcal{C})} \tag{4.15}$$

where $\mathcal{D}$ runs over all collections of j disjoint paths connecting sources from J with the sinks from $m+J$, $\mathcal{C}$ runs over all collections of disjoint cycles in the network on the cylinder, and $\operatorname{sgn}(\mathcal{D})$ is the sign of the permutation $\pi_{\mathcal{D}}$ of size j realized by the paths from the collection $\mathcal{D}$. Equation (4.15) takes into account that there are no contractible cycles in $\mathcal{N}$, and hence any cycle that survives on the cylinder intersects any path between a source and a sink. Consequently, the denominator in (4.15) equals $\mathfrak{P}_{\mathcal{N}}(\lambda, 0)$.

To proceed with the numerator, assume that $\pi_{\mathcal{D}}$ can be written as the product of c cycles of lengths $l_1, \dots, l_c$ subject to $l_1 + \cdots + l_c = j$. Then $\operatorname{sgn}(\pi_{\mathcal{D}}) = (-1)^{l_1-1}\cdots(-1)^{l_c-1} = (-1)^{j-c}$. It is easy to see that on the torus, the paths from $\mathcal{D}$ form exactly c disjoint cycles, and that the intersection index of the ith cycle with γ equals l_i. By (4.13)–(4.15), we can write

$$\det(I_m + zM(\lambda)) = \frac{\sum_{j=0}^{m} z^j \sum_{|J|=j}\sum_{\mathcal{C}}(-1)^j(-1)^{|\mathcal{C}|}\prod_{C\in\mathcal{C}}\bar{w}(C)}{\mathfrak{P}(\lambda,0)},$$

where the inner sum is taken over all collections $\mathcal{C}$ that intersect γ at the prescribed set J of points. Clearly, the numerator of the above expression equals $\mathfrak{P}_{\mathcal{N}}(\lambda, z)$, and (4.12) follows. □

Corollary 4.9. *One has*

$$\det(I_k + zM_{k,n}(\lambda)) = (1+z)\det(I_n + \lambda A_{k,n}(z)) = \mathfrak{P}_{\bar{\mathcal{N}}_{k,n}}(\lambda, z). \tag{4.16}$$

Proof. It is easy to see that the network $\bar{\mathcal{N}}_{k,n}$ does not have contractible cycles. Besides, both γ and ρ are ideal rims with respect to each other. Therefore, by Proposition 4.8,

$$\det(I_k + zM_{k,n}(\lambda)) = \frac{\mathfrak{P}_{\bar{\mathcal{N}}_{k,n}}(\lambda, z)}{\mathfrak{P}_{\bar{\mathcal{N}}_{k,n}}(\lambda, 0)}, \qquad \det(I_n + \lambda A_{k,n}(z)) = \frac{\mathfrak{P}_{\bar{\mathcal{N}}_{k,n}}(\lambda, z)}{\mathfrak{P}_{\bar{\mathcal{N}}_{k,n}}(0, z)}.$$

Next, the network $\mathcal{N}_{k.n}$ is acyclic, and so $\mathfrak{P}_{\bar{\mathcal{N}}_{k,n}}(\lambda, 0) = 1$. Finally, the weight of the only simple cycle in the conjugate network $\mathcal{N}'_{k,n}$ equals z, hence $\mathfrak{P}_{\bar{\mathcal{N}}_{k,n}}(0, z) = 1 + z$ and (4.16) follows. □

4.4. Lax representations

Another way to see the invariance of I_{ij} under T_k is based on a *zero curvature Lax representation* with a spectral parameter. A zero curvature representation for a non-linear dynamical system is a compatibility condition for an over-determined system of linear equations; this is a powerful method of establishing algebraic–geometric complete integrability, see, e.g., [7]. Even more generally, the term "Lax representation" is often used for discrete systems that can be described via a re-factorization of matrix rational functions $A(z) = A_1(z)A_2(z) \mapsto A^*(z) = A_2(z)A_1(z)$, see, e.g., [29].

Proposition 4.10. *The map T_k has a $k \times k$ zero curvature representation*

$$L_i^*(\lambda) = P_i(\lambda) L_{i+r-1}(\lambda) P_{i+1}^{-1}(\lambda)$$

and an $n \times n$ Lax representation

$$A_{k,n}(z) = A_1(z)A_2(z) \;\mapsto\; A^*_{k,n}(z) = A_2(z)A_1(z).$$

Here the Lax matrices $L_i(\lambda)$ and $A_{k,n}(z)$ are defined by (4.2) and (4.4), respectively, and $L_i^*(\lambda)$ and $A^*_{k,n}(z)$ are their images under the transformation T_k. The auxiliary matrix $P_i(\lambda)$ is given by

$$P_i(\lambda) = \begin{pmatrix} -\frac{x_{i-1}}{\sigma_{i-1}} - \frac{1}{\lambda\sigma_i} & \frac{1}{\lambda} \\ -\frac{1}{\sigma_i} & 0 \end{pmatrix}$$

for $k = 2$ and

$$P_i(\lambda) = \begin{pmatrix} 0 & -\frac{x_i}{\lambda\sigma_i} & -\frac{y_{i+1}}{\lambda\sigma_{i+1}} & 0 & \dots & 0 & 0 \\ 0 & 0 & \frac{x_{i+1}}{\sigma_{i+1}} & \frac{y_{i+2}}{\sigma_{i+2}} & \dots & 0 & 0 \\ \dots & \dots & \dots & \dots & \dots & \dots & \dots \\ 0 & 0 & 0 & \dots & \frac{x_{i+k-4}}{\sigma_{i+k-4}} & \frac{y_{i+k-3}}{\sigma_{i+k-3}} & 0 \\ -\frac{1}{\sigma_{i+k-2}} & 0 & 0 & \dots & 0 & \frac{x_{i+k-3}}{\sigma_{i+k-3}} & 1 \\ \frac{1}{\sigma_{i+k-2}} & \frac{1}{\lambda\sigma_{i+k-1}} & 0 & \dots & 0 & 0 & 0 \\ 0 & -\frac{1}{\lambda\sigma_{i+k-1}} & 0 & \dots & 0 & 0 & 0 \end{pmatrix},$$

for $k \geq 3$, where, as before, $\sigma_i = x_i + y_i$. Finally, $A_j(z)$ are given by

$$A_1(z) = ZD_\sigma(\mathbf{1}_n - Z)^{-1}Z^{-r'},$$
$$A_2(z) = Z^{r'+2}\left(D_x + ZD_y\right)D_\sigma^{-1}Z^{k-2}, \tag{4.17}$$

where $D_\sigma = D_x + D_y = \operatorname{diag}(\sigma_1, \ldots, \sigma_n)$.

Proof. The claim can be verified by a direct calculation using equations (3.8). It is worth pointing out, however, that expressions for $P_i(\lambda)$ and $A_j(z)$ were derived by re-casting elementary network transformations that constitute T_k as matrix transformation. We will provide an explanation for the $n \times n$ Lax representation and leave the details for the $k \times k$ Lax representation as an instructive exercise for an inquisitive reader.

First, we rewrite equation (3.8) for T_k in terms of D_x, D_y:

$$\begin{aligned} D_x^* &= \left(Z^{-r'-1}D_xD_\sigma^{-1}Z^{r'+1}\right)\left(Z^rD_\sigma Z^{-r}\right) \\ &= Z^{-r'-1}\left(D_xD_\sigma^{-1}\right)\left(Z^{k-1}D_\sigma Z^{1-k}\right)Z^{r'+1}, \\ D_y^* &= \left(Z^{-r'}D_yD_\sigma^{-1}Z^{r'}\right)\left(Z^{r+1}D_\sigma Z^{-r-1}\right) \\ &= Z^{-r'}\left(D_xD_\sigma^{-1}\right)\left(Z^{k-1}D_\sigma Z^{1-k}\right)Z^{r'}, \end{aligned}$$

which allows one to express $Z^{r'+1}A_{k,n}^*(z)Z^{-r'-1}$ as

$$Z\left(D_xD_\sigma^{-1}\left(Z^{k-1}D_\sigma Z^{1-k}\right)Z^{-1} + ZD_yD_\sigma^{-1}Z^{-1}\left(Z^kD_\sigma Z^{-k}\right)\right)Z^{k-1}\left(\mathbf{1}_n - Z\right)^{-1}.$$

Denote $Z^{r'+1}A_{k,n}^*(z)Z^{-r'-1}$ by $A_{k,n}^\sharp(z)$. If we find $A_1^\sharp(z)$, $A_2^\sharp(z)$ such that

$$A_{k,n}(z) = A_1^\sharp(z)A_2^\sharp(z), \qquad A_{k,n}^\sharp(z) = A_2^\sharp(z)A_1^\sharp(z),$$

then $A_1(z) = A_1^\sharp(z)Z^{-r'-1}$, $A_2(z) = A_2^\sharp(z)Z^{r'+1}$ will provide the desired Lax representation.

Consider the transformation of the network $\mathcal{N}'_{k,n}$ induced by performing type 3 Postnikov's move at all quadrilateral faces followed by performing type 1 Postnikov's move at all white–white edges. The resulting network is shown in Fig. 15.

To obtain a factorization of $A_{k,n}(z)$, we will view the latter network as a concatenation of two networks glued across a closed contour that intersects all white–white edges and no other edges (in Fig. 15 it is represented by the dashed circle). Intersection points are labeled 1 through n counterclockwise with the label i attached to the point in the white–white edge incident to the edge of weight σ_{i+1}. Furthermore, we adjusted the cut in such a way that it crosses the dashed circle through the segment between points labeled 1 and n.

Let $A_1^\sharp(z)$ and $A_2^\sharp(z)$ be boundary measurement matrices associated with the outer and the inner networks obtained this way. Clearly, $A_{k,n}(z) = A_1^\sharp(z)A_2^\sharp(z)$. To be able to perform the last sequence of transformation involved in T_k, namely to apply type 3

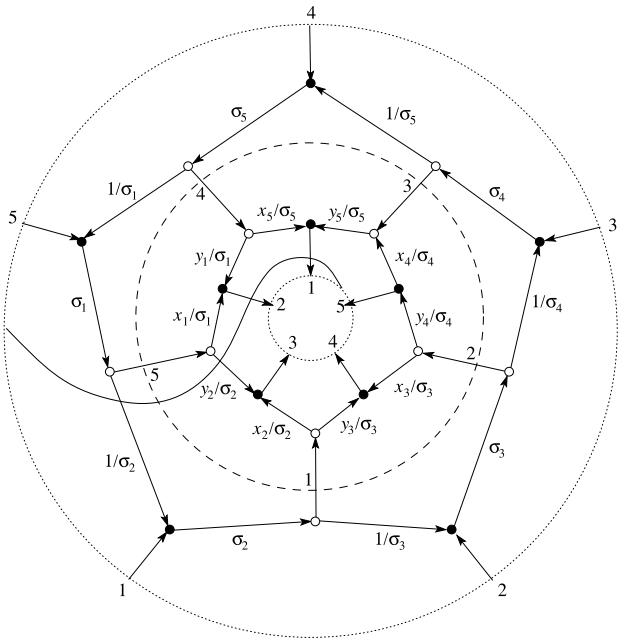

Fig. 15. The conjugate network $\mathcal{N}'_{3,5}$ after Postnikov's moves.

Postnikov's move to all black–black edges, we have to cut the torus in a different way: we first need to separate two networks along the dashed circle and then glue the outer boundary of the outer network to the inner boundary of the inner network matching the labels of boundary vertices. But this means that $A^\sharp_{k,n}(z) = A^\sharp_2(z)A^\sharp_1(z)$.

It remains to check that expressions for $A^\sharp_1(z)$, $A^\sharp_2(z)$ are consistent with (4.17). Note that the cut crosses the dashed circle between the intersection points labeled $n-r'-1$ and $n-r'$. The network that corresponds to $A^\sharp_1(z)$ contains a unique oriented cycle of weight z and, for any i,j, a unique simple directed path from source to sink j that contains the edge of weight σ_{i+1}. This path does not intersect the cut if $i \le j$, otherwise it intersects the cut once. Thus, the (i,j) entry of $A^\sharp_1(z)$ is equal $\frac{\sigma_{i+1}}{1+z}$ for $i \le j$ and $-\frac{\sigma_{i+1}z}{1+z}$ for $i > j$, which means that $A^\sharp_1(z) = ZD_\sigma Z^{-1}(\mathbf{1}_n - Z)^{-1}$ as needed.

The network that corresponds to $A^\sharp_2(z)$ contains no oriented cycles. The source i is connected by a directed path of weight x_i/σ_i to the sinks $i+k-1$ and by a directed path of weight y_{i+1}/σ_{i+1} to the sink $i+k$. The former path intersects the cut if and only if $n-k+2 \le i \le n$, and the latter path intersects the cut if and only if $n-k+1 \le i \le n$. We conclude that $A^\sharp_2(z) = Z\,(D_x + ZD_y)\,D_\sigma^{-1}Z^{k-2}$, as needed. □

In view of Proposition 4.10, the preservation of spectral invariants of $M_{k,n}(\lambda)$ (called, in this context, the *monodromy matrix*) and $A_{k,n}(\lambda)$ is obvious. In particular,

$$M^*_{k,n} = P_1 L_r \cdots L_n L_1 \cdots L_{r-1} P_1^{-1}.$$

Remark 4.11. 1. Two representations we obtained for T_k give an example of what in integrable systems literature is called *dual Lax representations*. A general technique for constructing integrable systems possessing such representations based on dual moment maps was developed in [1].

2. For $k = 3$, we obtain a 3×3 zero-curvature representation for the pentagram map alternative to the one given in [42].

4.5. Complete integrability

Theorem 4.12. *The map T_k is completely integrable for $k \geq 2$.*

Proof. Proposition 4.7 shows that spectral invariants of $M_{k,n}(\lambda)$ (equivalently, by Corollary 4.9, spectral invariants of $A_{k,n}(z)$) are conserved quantities for T_k, while Theorem 4.1 and Proposition 4.5 imply that conserved quantities Poisson-commute. To establish complete integrability, we need to prove that this Poisson-commutative family is maximal.

By Proposition 4.5, the number of Casimir functions for our Poisson structure is $2d$, where $d = \gcd(k-1, n)$. Therefore, we need to show that among spectral invariants of $A_{k,n}(z)$ there are $n + d$ independent functions of $\mathbf{x} = (x_i)_{i=1}^n$, $\mathbf{y} = (y_i)_{i=1}^n$. Furthermore, among Casimir functions described in (4.8) there are d independent functions that depend only on $\mathbf{y}$. Hence it suffices to prove that gradients of functions $f_s(\mathbf{x}, \mathbf{y}) = \frac{1}{s+1} \operatorname{Tr} A_{k,n}^{s+1}(z)$, $s = 0, \dots, n-1$, viewed as functions of $\mathbf{x}$ are linearly independent for almost all $\mathbf{x}, \mathbf{y}$ or, equivalently, since $f_s(\mathbf{x}, \mathbf{y})$ are polynomials, for at least one point $\mathbf{x}, \mathbf{y}$. Using the formula for variation of traces of powers of a square matrix

$$\delta \operatorname{Tr} A^{s+1} = \operatorname{Tr} \sum_{i=0}^{s} A^i \delta A A^{s-i} = (s+1) \operatorname{Tr}(\delta A A^s),$$

we deduce that the ith component of the gradient $\nabla_{\mathbf{x}} f_s(\mathbf{x}, \mathbf{y})$ with respect to $\mathbf{x}$ is equal to the ith diagonal element of the matrix

$$Z^{k-1}(\mathbf{1}_n - Z)^{-1} \left((D_x + D_y Z) Z^{k-1} (\mathbf{1}_n - Z)^{-1} \right)^s.$$

In particular,

$$\begin{aligned}
(\nabla_{\mathbf{x}} f_s(\mathbf{x}, -\mathbf{x}))_i &= \left(Z^{k-1}(\mathbf{1}_n - Z)^{-1} \left(D_x Z^{k-1} \right)^s \right)_{ii} \\
&= \frac{1}{1+z} \left(Z^{k-1}(\mathbf{1}_n + \ldots + Z^{n-1}) \left(D_x Z^{k-1} \right)^s \right)_{ii} \\
&= \frac{1}{1+z} \left(Z^{k-1+l} \left(D_x Z^{k-1} \right)^s \right)_{ii} \\
&= \frac{(-z)^{\lceil \frac{(s+1)(k-1)}{n} \rceil}}{1+z} \prod_{\beta=1}^{s} x_{i-\beta(k-1)}.
\end{aligned}$$

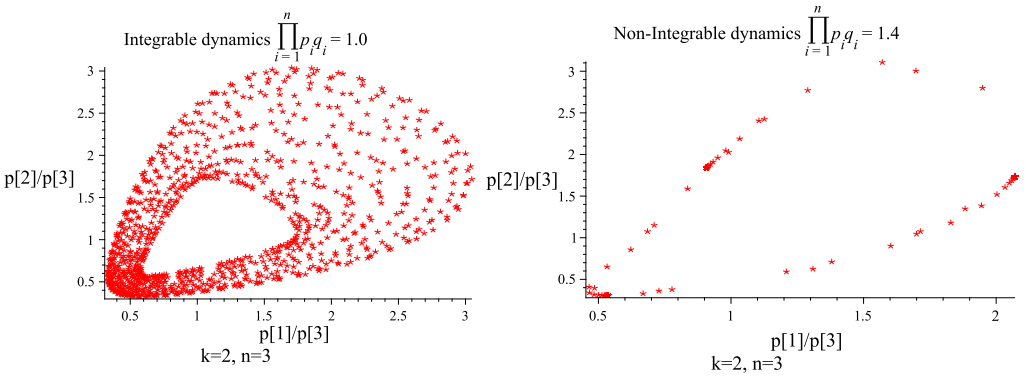

Fig. 16. Integrable and non-integrable dynamics.

Here the second line follows from (4.6), in the third line $l + (s+1)(k-1) = 0 \bmod n$, since only one of the powers of Z present in the second line contributes to the diagonal, and it is the one with the exponent divisible by n, the fourth line is obtained by repeated application of (4.5), and the index $i-\beta(k-1)$ is understood mod n. Prefactors depending on z play no role in analyzing linear independence of $\nabla_{\mathbf{x}} f_s(\mathbf{x}, -\mathbf{x})$, so we ignore them and form an $n \times n$ matrix $F = \left(\prod_{\beta=1}^{s} x_{i-\beta(k-1)}\right)_{s,i=1}^{n}$. We need to show that $\det F$ is generically nonzero. We further specialize by setting $x_{d+1} = \cdots = x_n = 1$, then columns of F become

$$F_{i+\alpha(k-1)} = \mathrm{col}(\underbrace{1, \ldots, 1}_{\alpha}, \underbrace{x_i, \ldots, x_i}_{n/d}, \underbrace{x_i^2, \ldots, x_i^2}_{n/d}, \ldots)$$

for $i = 1, \ldots, d$, $\alpha = 1, \ldots, n/d$. Now the standard argument (akin to the one used in computing Vandermonde determinants) shows that up to a sign $\det F$ is equal to $\prod_{i=1}^{d} (x_i - 1)^{n/d-1} \prod_{1 \le i < j \le d} (x_i - x_j)^{n/d}$. The proof is complete. □

Corollary 4.13. *Any rational function of I_{ij} that is homogeneous of degree zero in variables x, y, depends only on p, q and is preserved by the map $\overline{T}_k$. On the level set $\{\Pi p_i q_i = 1\}$, such functions generate a complete involutive family of integrals for the map $\overline{T}_k$.*

Remark 4.14. In general, these functions define a continuous integrable system on level sets of the form $\{\Pi p_i = c_1, \Pi q_i = c_2\}$, and the map $\overline{T}_k^{(c)}$ intertwines the flows of this system on different level sets lying on the same hypersurface $c_1 c_2 = c$. Numerical evidence suggests that $\overline{T}_k^{(c)}$ is not integrable whenever $c \neq 1$. Indeed, the left part of Fig. 16 demonstrates the typical integrable behavior while the right part clearly shows at least three accumulation points which contradicts integrability.

4.6. Spectral curve

We could have deduced independence of the integrals of T_k from the properties of the *spectral curve*

$$\begin{aligned}\mathfrak{P}_{\bar{\mathcal{N}}_{k,n}}(\lambda, z) &= \det(I_k + zM_{k,n})(\lambda)) = (1+z)\det(I_n + \lambda A_{k,n}(z)) \\ &= \sum_{i,j} I_{ij}\lambda^i z^j = 0 \end{aligned} \tag{4.18}$$

in the spirit of [30, Section 9]. We will briefly discuss this spectral curve here to point out parallels between our approach and that of [19]. There, the starting point for constructing an integrable system is a centrally symmetric polygon Δ with vertices in $\mathbb{Z}^2$ which gives rise to a dimer configuration on a torus whose *partition function* serves as a generating function for Casimirs and integrals in involution and defines an algebraic curve with a Newton polygon Δ.

Proposition 4.15. *The Newton polygon Δ of the spectral curve (4.18) is a parallelogram with vertices $(0,0), (0,1), (n,k), (n,k-1)$.*

Proof. Obviously, $(0,0), (0,1) \in \Delta$. Since

$$\det A_{k,n}(z) = \frac{(-z)^{k-1}}{1+z}\left(\prod_i x_i - (-1)^n z \prod_i y_i\right)$$

by (4.4), $(n,k), (n,k-1)$ are in Δ.

Let $(i,j) \in \Delta$; by the construction of $\mathfrak{P}_{\bar{\mathcal{N}}_{k,n}}(\lambda, z)$, it corresponds to a family $\mathcal{C}$ of disjoint simple cycles in $\bar{\mathcal{N}}_{k,n}$ that has in total i intersection points with ρ and j intersection points with γ. Consider a simple directed cycle $C_t \in \mathcal{C}$ that intersects the cut ρ at points numbered $\alpha_1, \dots, \alpha_{i_t+1} = \alpha_1$ (we list them in the order they appear along C_t starting with the smallest number and denote this list $A(C_t)$). It is convenient to visualize C_t using the network $\mathcal{N}'_{k,n}$. Then one can see that α_{s+1} can be expressed as $\alpha_{s+1} = \alpha_s + \beta_s \mod n$, where $s = 1, \dots, i_t$ and $\beta_s \in [k-1, n+k-2]$, see Fig. 14. We thus have $i_t(k-1) \le \beta_1 + \dots + \beta_{i_t} = j_t n$ for some j_t, which means that C_t intersects the rim γ exactly j_t times. Consequently, i_t and j_t are subject to the inequality $\frac{k-1}{n} i_t \le j_t$. Summing up over all cycles in $\mathcal{C}$ and taking into account that $\sum i_t = i$, $\sum j_t = j$, we get $\frac{k-1}{n} i \le j$.

On the other hand, each shift β_s as above prohibits at least $\beta_s - k$ indices from entering the set $A(C)$ for any cycle $C \in \mathcal{C}$; more exactly, if $\beta_s > k$ then the prohibited indices are $\alpha_s + k, \dots, \alpha_s + \beta_s - 1$, otherwise there are no such indices. So, totally at least $j_t n - i_t k$ indices are prohibited. Clearly, the sets of prohibited indices for distinct cycles are disjoint. Therefore, altogether at least $jn - ik$ indices are prohibited and i indices

are used, hence $jn - i(k-1) \le n$. Thus, if $(i,j) \in \Delta$, then $\frac{k-1}{n} i \le j \le \frac{k-1}{n} i + 1$, which, together with an obvious inequality $0 \le i \le n$, proves the claim. □

There are $2(d+1)$ integer points on the boundary of Δ:

$$\left(l\frac{n}{d}, l\frac{k-1}{d} \right), \qquad \left(l\frac{n}{d}, l\frac{k-1}{d} + 1 \right), \quad l = 0, \dots, d.$$

The number of interior integer points (equal to the genus of the spectral curve) is $n-d$. The coefficient of $\mathfrak{P}_{\bar{\mathcal{N}}_{k,n}}(\lambda, z)$ that corresponds to a point of the first type is a sum where each term is the product of weights of l disjoint cycles, each of them characterized uniquely by $i = n/d$, $\alpha_1 \in [1,d]$, and $\beta_1 = \ldots = \beta_{n/d} = k-1$ (see Fig. 14). The weight of such cycle is the Casimir function $\prod_{s=0}^{n/d-1} x_{\alpha_1 + s(k-1)}$, cp. with the first expression in (4.8).

On the other hand, any term contributing to the coefficient corresponding to a point of the second type is the weight of a collection of disjoint cycles that is represented in $\mathcal{N}'_{k,n}$ by a unique collection of non-intersecting paths joining ln/d sources $\alpha_1, \alpha_2, \dots, \alpha_l$, $\alpha_1 + (k-1), \alpha_2 + (k-1), \dots, \alpha_l + (k-1), \dots$ to sinks $\alpha_2 + (k-1), \alpha_3 + (k-1), \dots$, $\alpha_l + (k-1), \alpha_1 + 2(k-1), \dots$, respectively, where $1 \le \alpha_1 < \ldots < \alpha_l \le d$. The weight in question is the product of Casimir functions $\prod_{s=0}^{n/d-1} y_{\alpha_t + s(k-1)}$ for $t = 1, \dots, l$, cp. with the second expression in (4.8).

Thus, just like in [19], interior points of Δ correspond to independent integrals while integer points on the boundary of Δ correspond to Casimir functions.

5. Geometric interpretation

In this section we give a geometric interpretations of the maps T_k. The cases $k \ge 3$ and $k = 2$ are different and are treated separately.

5.1. The case $k \ge 3$

5.1.1. Corrugated polygons and generalized higher pentagram maps

As we already mentioned, a *twisted n-gon* in a projective space is a sequence of points $V = (V_i)$ such that $V_{i+n} = M(V_i)$ for all $i \in \mathbf{Z}$ and some fixed projective transformation M called the *monodromy*. The projective group naturally acts on the space of twisted n-gons. Let $\mathcal{P}_{k,n}$ be the space of projective equivalence classes of generic twisted n-gons in $\mathbf{RP}^{k-1}$, where "generic" means that every k consecutive vertices do not lie in a projective subspace. Clearly, the space $\mathcal{P}_{k,n}$ has dimension $n(k-1)$.

We say that a twisted polygon V is *corrugated* if, for every i, the vertices V_i, V_{i+1}, V_{i+k-1} and V_{i+k} span a projective plane. The projective group preserves the space of corrugated polygons. Projective equivalence classes of corrugated polygons constitute an algebraic subvariety of the moduli space of polygons in the projective space. Note that a polygon in $\mathbf{RP}^2$ is automatically corrugated.

Denote by $\mathcal{P}^0_{k,n} \subset \mathcal{P}_{k,n}$ the space of projective equivalence classes of corrugated polygons satisfying the additional genericity assumption that, for every i, every three out of the four vertices V_i, V_{i+1}, V_{i+k-1} and V_{i+k} are not collinear.

Lemma 5.1. *One has:* $\dim \mathcal{P}^0_{k,n} = 2n$.

Proof. As it was already mentioned, $\dim \mathcal{P}_{k,n} = n(k-1)$. For each $i = 1, \dots, n$, one has a constraint: the vertex V_{i+k} lies in the projective plane spanned by V_i, V_{i+1}, V_{i+k-1}. The codimension of a plane in $\mathbf{RP}^{k-1}$ is $k-3$, which yields $k-3$ equations. Thus

$$\dim \mathcal{P}^0_{k,n} = n(k-1) - n(k-3) = 2n,$$

as claimed. □

The consecutive $(k-1)$-*diagonals* (the diagonals connecting V_i and V_{i+k-1}) of a corrugated polygon intersect, and the intersection points form the vertices of a new twisted polygon: the ith vertex of this new polygon is the intersection of diagonals (V_i, V_{i+k-1}) and (V_{i+1}, V_{i+k}). This $(k-1)$-diagonal map commutes with projective transformations, and hence one obtains a rational map $F_k : \mathcal{P}^0_{k,n} \to \mathcal{P}_{k,n}$. (Note that this rational map is well defined only on an open subset of $\mathcal{P}^0_{k,n}$ because the image polygon may be degenerate.) F_3 is the pentagram map; the maps F_k for $k > 3$ are called *generalized higher pentagram maps*.

Remark 5.2. Corrugated polygons for $k > 2$ were independently defined by M. Glick (private communication).

Given a corrugated polygon V, one can also construct a new polygon whose ith vertex is the intersection of the lines (V_i, V_{i+1}) and (V_{i+k-1}, V_{i+k}). This defines a map $G_k : \mathcal{P}^0_{k,n} \to \mathcal{P}_{k,n}$.

Similarly to above, one can define spaces of twisted and corrugated polygons in the dual projective space $(\mathbf{RP}^{k-1})^*$, as well as dual analogs of the maps F_k and G_k; in what follows, the objects in the dual space will be marked by an asterisk. Besides, we will need the notion of the projectively dual polygon. Let V be a generic polygon in $\mathbf{RP}^{k-1}$. Each consecutive $(k-1)$-tuple of vertices spans a projective hyperplane, that is, a point of $(\mathbf{RP}^{k-1})^*$. This ordered collection of points represents the vertices of the dual polygon $W = V^*$; more exactly, the projective hyperplane spanned by $V_i, \dots, V_{i+k-2}$ represents the vertex W_i. We denote the projective duality map that takes V to W by Δ_k.

Proposition 5.3. (i) *The image of a corrugated polygon under F_k and under G_k is a corrugated polygon.*

(ii) *Up to a shift of indices by k, the maps F_k and G_k are inverse to each other.*

(iii) *The polygon projectively dual to a corrugated polygon is corrugated.*

(iv) *Projective duality Δ_k conjugates the maps F_k and G_k^*.*

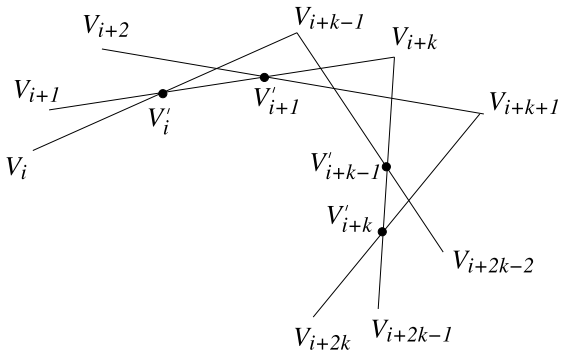

Fig. 17. The maps F_k and G_k.

Proof. (i) Let V'_i denote the ith vertex of $F_k(V)$. We claim that the vertices V'_i, V'_{i+1}, V'_{i+k-1}, V'_{i+k} lie in a projective plane. Indeed, V'_i and V'_{i+1} belong to the line (V_{i+1}, V_{i+k}), and V'_{i+k-1} and V'_{i+k} to the line (V_{i+2k-1}, V_{i+k}). These lines intersect at the point V_{i+k}, hence the points V'_i, V'_{i+1}, V'_{i+k-1}, V'_{i+k} are coplanar, see Fig. 17.

The argument for the map G_k is analogous.

(ii) Follows immediately from the definition of F_k and G_k, see Fig. 17.

(iii) Lift points in $\mathbf{RP}^{k-1}$ to vectors in $\mathbf{R}^k$; the lift is not unique and is defined up to a multiplicative factor. We use tilde to indicate a lift of a point. A lift of a twisted polygon is also twisted: $\widetilde{V}_{i+n} = \widetilde{M}(\widetilde{V}_i)$ for all i, where $\widetilde{M} \in GL(k, \mathbf{R})$ is a lift of the monodromy.

Fix a volume form in $\mathbf{R}^k$. Then $(k-1)$-vectors are identified with covectors. In particular, if $V_i, \dots, V_{i+k-2}$ are points in $\mathbf{RP}^{k-1}$ spanning a hyperplane then the respective point W_i of the dual space $(\mathbf{RP}^{k-1})^*$ lifts to $\widetilde{W}_i = \widetilde{V}_i \wedge \dots \wedge \widetilde{V}_{i+k-2}$.

Let V be a generic corrugated polygon. We need to prove that the $(k-1)$-vectors $\widetilde{W}_i$, $\widetilde{W}_{i+1}$, $\widetilde{W}_{i+k-1}$ and $\widetilde{W}_{i+k}$ are linearly dependent for all i.

Since the polygon V is corrugated, $\widetilde{V}_{i+2k-2} \in \operatorname{span}(\widetilde{V}_{i+2k-3}, \widetilde{V}_{i+k-2}, \widetilde{V}_{i+k-1})$, and hence

$$\widetilde{W}_{i+k} = \widetilde{V}_{i+k} \wedge \dots \wedge \widetilde{V}_{i+2k-2} \in \operatorname{span}(\widetilde{V}_{i+k-2} \wedge \widetilde{V}_{i+k} \wedge \dots \wedge \widetilde{V}_{i+2k-3}, \widetilde{W}_{i+k-1}).$$

In its turn,

$$\begin{aligned}\widetilde{V}_{i+k-2} \wedge \widetilde{V}_{i+k} \wedge \dots \wedge \widetilde{V}_{i+2k-3} &= \widetilde{V}_{i+k-3} \wedge \widetilde{V}_{i+k-2} \wedge \widetilde{V}_{i+k} \wedge \dots \wedge \widetilde{V}_{i+2k-4} = \dots \\ &= \widetilde{V}_{i+1} \wedge \dots \wedge \widetilde{V}_{i+k-2} \wedge \widetilde{V}_{i+k} \\ &\in \operatorname{span}(\widetilde{V}_i \wedge \dots \wedge \widetilde{V}_{i+k-2}, \widetilde{V}_{i+1} \wedge \dots \wedge \widetilde{V}_{i+k-1}).\end{aligned}$$

The latter two $(k-1)$-vectors are $\widetilde{W}_i$ and $\widetilde{W}_{i+1}$, as needed.

(iv) We need to prove that $G_k^* \circ \Delta_k = \Delta_k \circ F_k$.

As before, we argue about lifted vectors. Let $\widetilde{V}$ be a lifted polygon, and let W be the polygon dual to V. The vertices of a lift of the polygon $W'' = G_k^*(W)$ are represented

by vectors in $\operatorname{span}(\widetilde{W}_i, \widetilde{W}_{i+1}) \cap \operatorname{span}(\widetilde{W}_{i+k-1}, \widetilde{W}_{i+k})$. Let $\widetilde{W}_i''$ be a vector spanning this line. Then

$$\widetilde{W}_i'' = \alpha\widetilde{W}_i + \beta\widetilde{W}_{i+1} = \lambda\widetilde{W}_{i+k-1} + \mu\widetilde{W}_{i+k}$$

for some coefficients $\alpha, \beta, \lambda, \mu$. Using the definition of the points W_i, we have:

$$\begin{aligned}\widetilde{W}_i'' &= (\alpha\widetilde{V}_i \pm \beta\widetilde{V}_{i+k-1}) \wedge \widetilde{V}_{i+1} \wedge \ldots \wedge \widetilde{V}_{i+k-2} \\ &= (\lambda\widetilde{V}_{i+k-1} \pm \mu\widetilde{V}_{i+2k-2}) \wedge \widetilde{V}_{i+k} \wedge \ldots \wedge \widetilde{V}_{i+2k-3}. \end{aligned} \tag{5.1}$$

On the other hand, the vertex V_i' of $F_k(V)$ is the intersection point of the lines (V_i, V_{i+k-1}) and (V_{i+1}, V_{i+k}). Let $\widetilde{V}_i'$ be a lift of this point; then $\widetilde{V}_i' = s\widetilde{V}_{i+1} + t\widetilde{V}_{i+k}$ where s and t are coefficients. We want to show that $\Delta_k(V_i') = W_i''$, that is, using the identification of $(k-1)$-vectors with covectors, that $\widetilde{V}_i' \wedge \widetilde{W}_i'' = 0$. Indeed, in view of (5.1),

$$\begin{aligned}\widetilde{V}_i' \wedge \widetilde{W}_i'' = {} & s\widetilde{V}_{i+1} \wedge (\alpha\widetilde{V}_i \pm \beta\widetilde{V}_{i+k-1}) \wedge \widetilde{V}_{i+1} \wedge \ldots \wedge \widetilde{V}_{i+k-2} \\ & + t\widetilde{V}_{i+k} \wedge (\lambda\widetilde{V}_{i+k-1} \pm \mu\widetilde{V}_{i+2k-2}) \wedge \widetilde{V}_{i+k} \wedge \ldots \wedge \widetilde{V}_{i+2k-3} = 0,\end{aligned}$$

as claimed. □

Remark 5.4. Let us briefly mention a natural continuous analog of corrugated polygons and the generalized higher pentagram maps. A twisted curve in $\mathbf{RP}^{k-1}$ is a map $\gamma : \mathbf{R} \to \mathbf{RP}^{k-1}$ such that $\gamma(x+1) = M(\gamma(x))$ for all x where M is a fixed projective transformation. The projective group naturally acts on twisted curves, and one considers the projective equivalence classes.

A curve is called c-corrugated if the tangent lines at points $\gamma(x)$ and $\gamma(x+c)$ are coplanar (not skew) for all $x \in \mathbf{R}$. We claim that the line connecting points $\gamma(x)$ and $\gamma(x+c)$ envelops a new curve, $\bar{\gamma}(x)$. Indeed, the coplanarity condition implies that $\gamma(x+c) - \gamma(x) = u(x)\gamma'(x) + v(x)\gamma'(x+c)$ for some functions u and v. Then the envelope $\bar{\gamma}$ is given by the equation

$$\bar{\gamma}(x) = \frac{u(x)}{u(x)+v(x)}\gamma(x) + \frac{v(x)}{u(x)+v(x)}\gamma(x+c),$$

as can be easily verified by differentiation.

Thus we obtain a map $F_c : \gamma \mapsto \bar{\gamma}$. It is even easier to describe a map G_c defined by a c-corrugated curve γ: it is traced by the intersection points of the tangent lines at points $\gamma(x)$ and $\gamma(x+c)$. These maps commute with projective transformations. Of course, the notion of corrugated curve is interesting only when $k-1 \geq 3$.

An analog of Proposition 5.3 holds; in particular, $F_c(\gamma)$ is again a c-corrugated curve. The dynamics of the projective equivalence classes of corrugated curves under the transformations F_c and G_c is an interesting subject; we do not dwell on it here.

Remark 5.5. Paper [25] concerns a multi-dimensional version of the pentagram map, called the *dented* pentagram map. This map, denoted by T_m^d, acts on the projective equivalence classes of polygons in $\mathbf{RP}^d$. The new vertices are determined as the intersection points of consecutive d hyperplanes; these hyperplanes are spanned by the consecutive vertices of the polygon, from the kth to the $(k+d)$th, skipping the $(k+m)$th vertex, where the index k takes d consecutive values. The standard pentagram map corresponds to the case when $d = 2$ and $m = 1$.

It is proved in [25] that the maps T_m^d, $m = 1, \dots, d-1$, are integrable in the sense that they admit a Lax representation with a spectral parameter. It is also observed that the restriction of these maps, for each m in the above range, to the space of corrugated polygons coincides with the map studied in the present paper. Furthermore, a broader class of polygons, called *partially corrugated*, is described, and complete integrability result is extended to this class. Paper [25] also contains a description of a continuous limit of the dented pentagram maps.

5.1.2. Coordinates in the space of corrugated polygons

Now we introduce coordinates in $\mathcal{P}_{k,n}^0$.

Proposition 5.6. *One can lift the vertices of a generic corrugated polygon V so that, for all i, one has:*

$$\widetilde{V}_{i+k} = y_{i-1}\widetilde{V}_i + x_i\widetilde{V}_{i+1} + \widetilde{V}_{i+k-1}, \tag{5.2}$$

where x_i and y_i are n-periodic sequences. Conversely, n-periodic sequences x_i and y_i uniquely determine the projective equivalence class of a twisted corrugated n-gon in $\mathbf{RP}^{k-1}$.

Proof. Consider a lifted twisted polygon $\widehat{V}$. Since V is corrugated, one has

$$\widehat{V}_{i+k} = a_{i+k-1}\widehat{V}_{i+k-1} + b_{i+1}\widehat{V}_{i+1} + c_i\widehat{V}_i \tag{5.3}$$

for all i. The sequences a_i, b_i and c_i are n-periodic and, due to the genericity assumption, none of these coefficients vanish.

We wish to choose the lift in such a way that the coefficient a identically equals 1. Rescale: $\widehat{V}_i = \lambda_i\widetilde{V}_i$, where $\lambda_i \neq 0$. Then for (5.3) to become (5.2), the following recurrence should hold for the scaling factors: $\lambda_{i+1} = a_i\lambda_i$. Set $\lambda_0 = 1$ and determine λ_i, $i \in \mathbf{Z}$, by the recurrence.

After this rescaling, the coefficients change as follows:

$$c_i \mapsto \frac{c_i}{a_i a_{i+1} \cdots a_{i+k-1}}, \qquad b_{i+1} \mapsto \frac{b_{i+1}}{a_{i+1} \cdots a_{i+k-1}}.$$

Hence

$$x_i = \frac{b_{i+1}}{a_{i+1}\cdots a_{i+k-1}}, \qquad y_i = \frac{c_{i+1}}{a_{i+1}\cdots a_{i+k}}. \tag{5.4}$$

Thus we obtain recurrence (5.2) with n-periodic coefficients uniquely determined by the projective equivalence class of the twisted corrugated polygon.

Conversely, given n-periodic sequences x_i and y_i, choose a frame $\widetilde{V}_0, \dots, \widetilde{V}_{k-1}$ in $\mathbf{R}^k$ and use recurrence (5.2) to construct a bi-infinite sequence of vectors $\widetilde{V}_i$. The periodicity of the sequences x_i and y_i implies that the polygon $\widetilde{V}$ is twisted, and relation (5.2) implies that it is corrugated. A different choice of a frame results in a linearly equivalent polygon and, after projection to $\mathbf{RP}^{k-1}$, in a projectively equivalent polygon V. □

The next theorem interprets the map T_k as the generalized higher pentagram map F_k.

Theorem 5.7. (i) *In the $(\mathbf{x}, \mathbf{y})$-coordinates, the maps F_k and G_k coincide with T_k and T_k^{-1} up to a shift of indices. More exactly, if $S_t : \mathcal{P}^0_{k,n} \to \mathcal{P}^0_{k,n}$ is the shift by t in the positive direction, then $F_k = T_k \circ S_{r'+1}$ and $G_k = T_k^{-1} \circ S_{r+1}$.*

(ii) *In the $(\mathbf{x}, \mathbf{y})$-coordinates, the projective duality Δ_k coincides with D_k up to a sign and a shift of indices. More exactly, $\Delta_k = (-1)^k D_k \circ S_{r'}$.*

Proof. (i) Let $\widetilde{V}$ be a polygon in $\mathbf{R}^k$ satisfying (5.2). Then

$$\widetilde{V}_{j+k-1} + y_{j-1}\widetilde{V}_j = \widetilde{V}_{j+k} - x_j\widetilde{V}_{j+1}$$

for $j = i, i+1, i+k-1, i+k$. It follows that, as lifts of points V'_i, V'_{i+1}, V'_{i+k-1}, V'_{i+k} in Fig. 17, one may set:

$$\begin{aligned} \widetilde{V}'_i &= \widetilde{V}_{i+k} - x_i\widetilde{V}_{i+1}, & \widetilde{V}'_{i+1} &= \widetilde{V}_{i+k} + y_i\widetilde{V}_{i+1}, \\ \widetilde{V}'_{i+k-1} &= \widetilde{V}_{i+2k-1} - x_{i+k-1}\widetilde{V}_{i+k}, & \widetilde{V}'_{i+k} &= \widetilde{V}_{i+2k-1} + y_{i+k-1}\widetilde{V}_{i+k}. \end{aligned} \tag{5.5}$$

One has a linear relation

$$\widetilde{V}'_{i+k} = a\widetilde{V}'_{i+k-1} + b\widetilde{V}'_{i+1} + c\widetilde{V}'_i.$$

Substitute from (5.5) to obtain

$$\widetilde{V}_{i+2k-1} + y_{i+k-1}\widetilde{V}_{i+k} = a(\widetilde{V}_{i+2k-1} - x_{i+k-1}\widetilde{V}_{i+k}) + b(\widetilde{V}_{i+k} + y_i\widetilde{V}_{i+1}) + c(\widetilde{V}_{i+k} - x_i\widetilde{V}_{i+1})$$

and use linear independence of the vectors $\widetilde{V}_{i+1}$, $\widetilde{V}_{i+k}$, $\widetilde{V}_{i+2k-1}$ to conclude that

$$a = 1, \qquad b = x_i\frac{x_{i+k-1} + y_{i+k-1}}{x_i + y_i}, \qquad c = y_i\frac{x_{i+k-1} + y_{i+k-1}}{x_i + y_i}.$$

Thus the vectors $\widetilde{V}_i'$, $\widetilde{V}_{i+1}'$, $\widetilde{V}_{i+k-1}'$, $\widetilde{V}_{i+k}'$ satisfy recurrence (5.2) with the coefficients

$$x_i' = x_i \frac{x_{i+k-1} + y_{i+k-1}}{x_i + y_i}, \qquad y_i' = y_{i+1} \frac{x_{i+k} + y_{i+k}}{x_{i+1} + y_{i+1}}.$$

This differs from (3.8) only by shifting indices by $r' + 1$.

The statement about G_k follows immediately from $F_k = T_k \circ S_{r'+1}$ and Proposition 5.3(ii).

(ii) We use the same notation as in Proposition 5.3. Let $\widetilde{V}$ be a polygon in $\mathbf{R}^k$ satisfying (5.2), and $\widetilde{W}$ be a lift of the dual polygon.

Going by the proof of Proposition 5.3(iii), line by line, we obtain the equalities:

$$\widetilde{W}_{i+k} = (-1)^k y_{i+k-3} \widetilde{V}_{i+k-2} \wedge \widetilde{V}_{i+k} \wedge \cdots \wedge \widetilde{V}_{i+2k-3} + (-1)^k x_{i+k-2} \widetilde{W}_{i+k-1},$$

and

$$\widetilde{V}_{i+k-2} \wedge \widetilde{V}_{i+k} \wedge \cdots \wedge \widetilde{V}_{i+2k-3} = (-1)^k y_{i-1} \cdots y_{i+k-4} \widetilde{W}_i + y_i \cdots y_{i+k-4} \widetilde{W}_{i+1}.$$

Hence

$$\widetilde{W}_{i+k} = (-1)^k x_{i+k-2} \widetilde{W}_{i+k-1} + (-1)^k y_i \cdots y_{i+k-3} \widetilde{W}_{i+1} + y_{i+1} \cdots y_{i+k-3} \widetilde{W}_i.$$

Using formulas (5.4), we find

$$x_i^* = (-1)^k \frac{y_i \cdots y_{i+k-3}}{x_i \cdots x_{i+k-2}}, \qquad y_i^* = (-1)^k \frac{y_i \cdots y_{i+k-2}}{x_i \cdots x_{i+k-1}},$$

which differs from (3.10) only by the sign and the shift of indices by r'. □

Remark 5.8. 1. In view of Theorem 5.7 and Proposition 3.7(i), (ii), we may identify the maps T_k° and G_k^*.

2. It would be interesting to provide a geometric interpretation for Proposition 3.7(iii), which connects the maps G_k^* and F_{n-k+2}.

Statement (i) of Theorem 5.7, along with Theorem 4.12, implies that the generalized higher pentagram map F_k is completely integrable.

Integrals of the pentagram map (1.1) were constructed by R. Schwartz in [38]. He observed that the map commutes with the scaling

$$X_i \mapsto \lambda X_i, \quad Y_i \mapsto \lambda^{-1} Y_i,$$

and that the conjugacy class of the monodromy of a twisted polygon is invariant under the map. Decomposing the characteristic polynomial of the monodromy into the homogeneous components with respect to the scaling, yields the integrals.

The next proposition shows that the integrals of the generalized higher pentagram map can be constructed in a similar way.

Proposition 5.9. *The integrals of F_k can be obtained from the monodromy M as the homogeneous components of its characteristic polynomial.*

Proof. By Theorem 5.7 and (4.11), it suffices to check that the matrix $M_{k,n}(\lambda)$ given by (4.3) is conjugate-transpose to the scaled monodromy $M(\lambda)$ of the respective twisted corrugated polygon.

Let us start with the monodromy. We use vectors $\widetilde{V}_1, \dots, \widetilde{V}_k$ as a basis in the vector space $\mathbf{R}^k$, and express the next vectors using (5.2). When we come to $\widetilde{V}_{n+1}, \dots, \widetilde{V}_{n+k}$, we get the monodromy matrix as a function of the coordinates $\mathbf{x}, \mathbf{y}$. This process is represented by the product of matrices $Q_i(\lambda)$ that encode one step $(\widetilde{V}_i, \dots, \widetilde{V}_{i+k-1}) \mapsto (\widetilde{V}_{i+1}, \dots, \widetilde{V}_{i+k})$. By (5.2)

$$Q_i(\lambda) = \begin{pmatrix} 0 & 1 & 0 & \dots & 0 & 0 \\ 0 & 0 & 1 & \dots & 0 & 0 \\ \dots & \dots & \dots & \dots & \dots & \dots \\ 0 & 0 & 0 & \dots & 0 & 1 \\ \lambda y_{i-1} & \lambda x_i & 0 & \dots & 0 & 1 \end{pmatrix},$$

where λ is the scaling factor, and $M(\lambda) = Q_n(\lambda)Q_{n-1}(\lambda)\cdots Q_1(\lambda)$.

Now consider $M_{k,n}(\lambda)^T$: by (4.3), it is the product of $L_i(\lambda)^T$, $i = 1, \dots, n$, in the reverse order, with $L_i(\lambda)$ given by (4.2). Let $A_i(\lambda)$ be an auxiliary matrix

$$A_i(\lambda) = \begin{pmatrix} \lambda^{-1} & 0 & 0 & \dots & 0 & 0 \\ 0 & 1 & 0 & \dots & 0 & 0 \\ 0 & 0 & 1 & \dots & 0 & 0 \\ \dots & \dots & \dots & \dots & \dots & \dots \\ x_i & 0 & 0 & \dots & 0 & 1 \end{pmatrix},$$

then $L_i(-\lambda)^T = A_{i+1}(\lambda)^{-1}Q_{i+1}(\lambda)A_i(\lambda)$, and hence

$$M_{k,n}(-\lambda)^T = A_{n+1}(\lambda)^{-1}Q_{n+1}(\lambda)q_n(\lambda)\cdots Q_2(\lambda)A_1(\lambda).$$

Taking into account that sequences $Q_i(\lambda)$ and $A_i(\lambda)$ are n-periodic by Proposition 5.6, we get

$$M_{k,n}(-\lambda)^T = A_1(\lambda)^{-1}Q_1(\lambda)M(\lambda)Q_1(\lambda)^{-1}A_1(\lambda),$$

and the claim follows. □

We complete the discussion of coordinates in the space of corrugated polygons by showing that the coordinates (p_i, q_i) introduced in Section 2 can be interpreted as cross-ratios of quadruples of collinear points. We use the following definition of cross-ratio (out of six possibilities):

$$[a, b, c, d] = \frac{(a-b)(c-d)}{(a-d)(b-c)}. \tag{5.6}$$

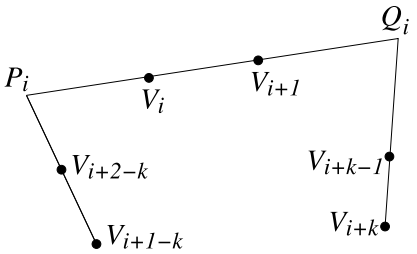

Fig. 18. Cross-ratios q_i.

To a twisted corrugated n-gon V we assign two n-periodic sequences of cross-ratios. Consider Fig. 17 and Fig. 18 (depicting the map G_k) and observe quadruples of collinear points. Their cross-ratios are related to the coordinates (p_i, q_i) as follows.

Proposition 5.10. *One has:*

$$p_i = [V_{i+1}, V_i', V_{i+k}, V_{i+1}'], \qquad q_{i-r-1} = [P_i, V_{i+1}, Q_i, V_i]$$

subject to $\prod_{i=1}^{n} p_i q_i = 1$.

Proof. Consider the lifted polygons. We saw in the proof of Theorem 5.7 that

$$\widetilde{V}_i' = \widetilde{V}_{i+k} - x_i \widetilde{V}_{i+1}, \quad \widetilde{V}_{i+1}' = \widetilde{V}_{i+k} + y_i \widetilde{V}_{i+1}.$$

Choose the basis in the 2-plane so that $\widetilde{V}_{i+1} = (1, 0)$, $\widetilde{V}_{i+k} = (0, 1)$. Then $\widetilde{V}_i' = (-x_i, 1)$, $\widetilde{V}_{i+1}' = (y_i, 1)$, and

$$[V_{i+1}, V_i', V_{i+1}', V_{i+k}] = [\infty, -x_i, 0, y_i] = \frac{y_i}{x_i} = p_i,$$

the last equality due to Proposition 3.3(ii).

Likewise, one has

$$P_i = \widetilde{V}_{i+1} - \widetilde{V}_i, \qquad Q_i = x_i \widetilde{V}_{i+1} + y_{i-1} \widetilde{V}_i$$

in Fig. 18, and this yields

$$[P_i, V_{i+1}, Q_i, V_i] = \frac{x_i}{y_{i-1}} = q_{i-r-1},$$

the last equality again due to Proposition 3.3(ii).

The condition on the product of all coordinates follows immediately. □

5.1.3. Higher pentagram maps on plane polygons

One also has the *skip* $(k-2)$*-diagonal map* on twisted polygons in the projective plane. Assume that the polygons are generic in the following sense: for every i, no three out of the four vertices V_i, V_{i+1}, V_{i+k-1} and V_{i+k} are collinear. The skip $(k-2)$-diagonal map assigns to a twisted n-gon V the twisted n-gon whose consecutive vertices are the intersection points of the lines (V_i, V_{i+k-1}) and (V_{i+1}, V_{i+k}). We call these maps *higher pentagram maps* and denote them by $\bar{F}_k$. Assume that the ground field is $\mathbf{C}$.

Arguing as in the proof of Proposition 5.6, we lift the points V_i to vectors $\widetilde{V}_i \in \mathbf{C}^3$ so that (5.2) holds. This provides a rational map ψ from the moduli space of twisted polygons in $\mathbf{CP}^2$ to the $(\mathbf{x}, \mathbf{y})$-space, that is, to the moduli space of corrugated twisted polygons in $\mathbf{CP}^{k-1}$. On the latter space, the generalized higher pentagram map F_k acts. The relation between these maps is as follows.

Proposition 5.11. (i) *The map ψ is $\binom{k}{3}$-to-one.*

(ii) *The map ψ conjugates $\bar{F}_k$ and F_k, that is, $\psi \circ \bar{F}_k = F_k \circ \psi$.*

Proof. Given periodic sequences x_i, y_i, we wish to reconstruct a twisted n-gon in $\mathbf{C}^3$, up to a linear equivalence. To this end, let the first three vectors $\widetilde{V}_1$, $\widetilde{V}_2$, $\widetilde{V}_3$ form a basis, and choose $\widetilde{V}_4, \dots, \widetilde{V}_k$ arbitrarily, so far. Then $\widetilde{V}_{k+1}$, and all the next vectors, are determined by the recurrence (5.2). The monodromy $\widetilde{M}$ is determined by the condition that

$$\widetilde{M}(\widetilde{V}_1) = \widetilde{V}_{n+1}, \quad \widetilde{M}(\widetilde{V}_2) = \widetilde{V}_{n+2}, \quad \widetilde{M}(\widetilde{V}_3) = \widetilde{V}_{n+3}. \tag{5.7}$$

The twist condition is that

$$\widetilde{M}(\widetilde{V}_j) = \widetilde{V}_{n+j}, \quad j = 4, \dots, k. \tag{5.8}$$

If this holds, then $\widetilde{M}(\widetilde{V}_i) = \widetilde{V}_{n+i}$ for all i. Note that (5.8) gives $3(k-3)$ equations on that many variables (the unknown vectors being $\widetilde{V}_4, \dots, \widetilde{V}_k$). We shall see that these are quadratic equations and proceed to solving them.

The recurrence (5.2) implies that $\widetilde{V}_q = \sum_{i=1}^{k} F_q^i \widetilde{V}_i$ where F_q^i is a function of $\mathbf{x}, \mathbf{y}$. One has: $\widetilde{V}_j = v_j^1 \widetilde{V}_1 + v_j^2 \widetilde{V}_2 + v_j^3 \widetilde{V}_3$ where v_j^1, v_j^2, v_j^3 are the components of the vector $\widetilde{V}_j$ in the basis $\widetilde{V}_1, \widetilde{V}_2, \widetilde{V}_3$. Rewrite (5.8), using (5.7), as

$$v_j^1 \left(\sum_{i=1}^{k} F_{n+1}^i \widetilde{V}_i \right) + v_j^2 \left(\sum_{i=1}^{k} F_{n+2}^i \widetilde{V}_i \right) + v_j^3 \left(\sum_{i=1}^{k} F_{n+3}^i \widetilde{V}_i \right) = \sum_{i=1}^{k} F_{n+j}^i \widetilde{V}_i,$$

or

$$A(\widetilde{V}_j) + \sum_{i=4}^{k} (F^i \cdot \widetilde{V}_j) \widetilde{V}_i = C_j + \sum_{i=4}^{k} g_j^i \widetilde{V}_i, \quad j = 4, \dots, k,$$

where $A = (F^{\beta}_{n+\alpha})$, $\alpha, \beta = 1, 2, 3$, is a 3×3 matrix, $F^i = (F^i_{n+1}, F^i_{n+2}, F^i_{n+3})$, $C_j = (F^1_{n+j}, F^2_{n+j}, F^3_{n+j})$, and $g^i_j = F^i_{n+j}$. Rewrite, once again, as

$$A(\widetilde{V}_j) - C_j = \sum_{i=4}^{k} [g^i_j - (F^i \cdot \widetilde{V}_j)]\ \widetilde{V}_i. \tag{5.9}$$

Let B be the $k \times k$ matrix that has A in the upper left corner, the vectors $-C_4, -C_5, \dots, -C_k$ to the right of A, the vectors $-(F_4)^t, \dots, -(F_k)^t$ below A, and the $(k-3)\times(k-3)$ matrix $G = g^i_j$ in the bottom right corner. The entries of B are functions of $\mathbf{x}, \mathbf{y}$. Let ξ_j, $j = 4, \dots, k$, be the k-dimensional vector $(V^1_j, V^2_j, V^3_j, 0, \dots, 0, 1, 0, \dots, 0)$ with 1 at jth position. Let $\mathcal{V}$ be the span of ξ_j, $j = 4, \dots, k$.

Claim. *The system (5.9) is equivalent to the condition that $\mathcal{V}$ is a B-invariant subspace, that is, a fixed point of the action of B on the Grassmannian* $\mathrm{Gr}(k-3, k)$.

Indeed, one has:

$$B(\xi_j) = (A(\widetilde{V}_j) - C_j, g^4_j - (F^4 \cdot \widetilde{V}_j), \dots, g^k_j - (F^k \cdot \widetilde{V}_j)). \tag{5.10}$$

If (5.9) holds then

$$\begin{aligned} B(\xi_j) &= \left(\sum_{i=4}^{k} [g^i_j - (F^i \cdot \widetilde{V}_j)]\ \widetilde{V}_i, g^4_j - (F^4 \cdot \widetilde{V}_j), \dots, g^k_j - (F^k \cdot \widetilde{V}_j) \right) \\ &= \sum_{i=4}^{k} [g^i_j - (F^i \cdot \widetilde{V}_j)]\ \xi_i, \end{aligned}$$

so $\mathcal{V}$ is B-invariant.

Conversely, if $\mathcal{V}$ is B-invariant then $B(\xi_j) = \sum_{i=4}^{k} \alpha_i \xi_i$ with some coefficients α_i. It follows from (5.10) that $\alpha_i = g^i_j - (F^i \cdot \widetilde{V}_j)$, and that

$$A(\widetilde{V}_j) - C_j = \sum_{i=4}^{k} [g^i_j - (F^i \cdot \widetilde{V}_j)] \widetilde{V}_i,$$

which is equation (5.9). This proves the claim.

A generic linear transformation B has a simple spectrum and k one-dimensional eigenspaces. One has $\binom{k}{3}$ invariant $(k-3)$-dimensional subspaces that can be parameterized as $\mathrm{span}(\xi_4, \dots, \xi_k)$. Thus one has $\binom{k}{3}$ choices of vectors $\widetilde{V}_4, \dots, \widetilde{V}_k$ for given coordinates x_i, y_i. In other words, the mapping ψ from the moduli space of twisted n-gons $\mathcal{P}_n$ to the $\mathbf{x}, \mathbf{y}$-space is $\binom{k}{3}$-to-one. That this map conjugates the skip $(k-2)$-diagonal map $\bar{F}_k$ with the map F_k is obvious, and we are done. □

It follows that if I is an integral of the map F_k then $I \circ \psi$ is an integral of the map $\bar{F}_k$. Thus the integrals (4.11) provide integrals of the higher pentagram map.

5.2. The case $k = 2$: leapfrog map and circle pattern

As we saw, for $k \geq 3$, one can define the pentagram map on individual polygons (and not only on the projective equivalence classes). The dynamics of this "lifted" map is not completely integrable; for example, if $k = 3$, the polygon exponentially fast shrinks to a point. Likewise, in the case $k = 2$, one can lift the map T_2 to individual polygons in the projective line. In this subsection we describe the geometry of this transformation; we do this in three ways, via projective, hyperbolic, and Möbius geometry.

5.2.1. Space of pairs of twisted n-gons in $\mathbf{RP}^1$

Let $\mathcal{S}_n$ be the space whose points are pairs of twisted n-gons (S^-, S) in $\mathbf{RP}^1$ with the same monodromy. Here S is a sequence of points $S_i \in \mathbf{RP}^1$, and likewise for S^-. One has: $\dim \mathcal{S}_n = 2n + 3$. The group $PGL(2, \mathbf{R})$ acts on $\mathcal{S}_n$. Let φ be the map from $\mathcal{S}_n$ to the $(\mathbf{x}, \mathbf{y})$-space given by the formulas:

$$x_i = \frac{(S_{i+1} - S^-_{i+2})(S^-_i - S^-_{i+1})}{(S^-_i - S_{i+1})(S^-_{i+1} - S^-_{i+2})},$$
$$y_i = \frac{(S^-_{i+1} - S_{i+1})(S^-_{i+2} - S_{i+2})(S^-_i - S^-_{i+1})}{(S^-_{i+1} - S_{i+2})(S^-_i - S_{i+1})(S^-_{i+1} - S^-_{i+2})}. \tag{5.11}$$

Recall that we use the cross-ratio defined by formula (5.6).

Proposition 5.12. (i) *The composition of φ with the projection π is given by the formulas*

$$p_i = [S^-_{i+1}, S_{i+1}, S^-_{i+2}, S_{i+2}], \quad q_i = \frac{[S^-_i, S_{i+1}, S_{i+2}, S^-_{i+3}][S^-_{i+1}, S^-_{i+2}, S_{i+2}, S^-_{i+3}]}{[S^-_i, S^-_{i+1}, S^-_{i+2}, S^-_{i+3}][S^-_{i+1}, S_{i+1}, S_{i+2}, S^-_{i+3}]}.$$

(ii) *The image of the map $\pi \circ \varphi$ belongs to the hypersurface $\prod_{i=1}^n p_i q_i = 1$.*

(iii) *The fibers of this maps are the $PGL(2, \mathbf{R})$-orbits, and hence the $(\mathbf{x}, \mathbf{y})$-space is identified with the moduli space $\mathcal{S}_n / PGL(2, \mathbf{R})$.*

Proof. (i) From Proposition 3.3, we have:

$$p_i = \frac{y_i}{x_i}, \qquad q_i = \frac{x_{i+1}}{y_i}. \tag{5.12}$$

Then a direct computation using formulas (5.11) for x and y yields the result.

(ii) The sequences x_i and y_i are n-periodic. Multiplying p_i and q_i from (5.12), $i = 1, \dots, n$, the numerators and denominators cancel out, and the result follows.

(iii) Put the sequences of points S^-, S in the interlacing order:

$$\dots, S^-_i, S_i, S^-_{i+1}, S_{i+1}, S^-_{i+2}, \dots$$

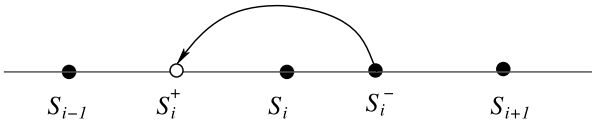

Fig. 19. Evolution of points in the projective line.

and consider the cross-ratios of the consecutive quadruples:

$$p_{i-1} = [S_i^-, S_i, S_{i+1}^-, S_{i+1}], \qquad r_i = [S_i, S_{i+1}^-, S_{i+1}, S_{i+2}^-];$$

the first equality was proved in (i), and the second is the definition of r. The sequences p_i and r_i are n-periodic and they determine the projective equivalence class of the pair (S^-, S). Thus we have a coordinate system $(\mathbf{p}, \mathbf{r})$ on $\mathcal{S}_n/PGL(2, \mathbf{R})$.

We wish to show that $(\mathbf{x}, \mathbf{y})$ is another coordinate system. Indeed, one can express $(\mathbf{x}, \mathbf{y})$ in terms of $(\mathbf{p}, \mathbf{r})$ and vice versa:

$$x_i = \frac{r_i(1+p_{i-1})}{1+r_i}, \quad y_i = \frac{r_i p_i(1+p_{i-1})}{1+r_i}; \qquad p_i = \frac{y_i}{x_i}, \quad r_i = \frac{x_{i-1}x_i}{x_{i-1}(1-x_i)+y_{i-1}}$$

(we omit this straightforward computation). □

5.2.2. Leapfrog transformation

Define a transformation Φ of the space $\mathcal{S}_n$, acting as $\Phi(S^-, S) = (S, S^+)$, where S^+ is given by the following local "leapfrog" rule: given a quadruple of points $S_{i-1}, S_i^-, S_i, S_{i+1}$, the point S_i^+ is the result of applying to S_i^- the unique projective involution that fixes S_i and interchanges S_{i-1} and S_{i+1}. Clearly, Φ commutes with projective transformations.

The transformation Φ can be defined this way over any ground field, however in $\mathbf{RP}^1$ we can interpret the point S_i^+ as the reflection of S_i^- in S_i in the projective metric on the segment $[S_{i-1}, S_{i+1}]$, whence the name; see Fig. 19. Recall that the projective metric on a segment is the Riemannian metric whose isometries are the projective transformations preserving the segment, see [5, Chap. 4]. That is, the projective distance between points P and Q on a segment AB is as given by the formula

$$d(P, Q) = \frac{1}{2} \ln \frac{(Q-A)(B-P)}{(P-A)(B-Q)}$$

(this formula defines distance in the Cayley–Klein, or projective, model of hyperbolic geometry; the factor $1/2$ is needed for the curvature to be -1).

Theorem 5.13. (i) *The map Φ is given by the following equivalent equations:*

$$\frac{1}{S_i^+ - S_i} + \frac{1}{S_i^- - S_i} = \frac{1}{S_{i+1} - S_i} + \frac{1}{S_{i-1} - S_i}, \tag{5.13}$$

$$\frac{(S_i^+ - S_{i+1})(S_i - S_i^-)(S_i - S_{i-1})}{(S_i^+ - S_i)(S_{i+1} - S_i)(S_i^- - S_{i-1})} = -1, \tag{5.14}$$

$$\frac{(S_i^+ - S_{i-1})(S_i - S_i^-)(S_{i+1} - S_i)}{(S_i^+ - S_i)(S_i - S_{i-1})(S_i^- - S_{i+1})} = -1. \tag{5.15}$$

(ii) *The map induced by* Φ *on the moduli space* $\mathcal{S}_n/PGL(2,\mathbf{R})$ *is the map* T_2 *given in* (3.8).

Proof. (i) A fractional–linear involution $x \mapsto y$ with a fixed point a is given by the formula

$$\frac{1}{x-a} + \frac{1}{y-a} = b$$

where b is some constant. Since the leapfrog involution has S_i as a fixed point and swaps S_i^- with S_i^+ and S_{i-1} with S_{i+1}, one has

$$\frac{1}{S_i^- - S_i} + \frac{1}{S_i^+ - S_i} = b = \frac{1}{S_{i-1} - S_i} + \frac{1}{S_{i+1} - S_i},$$

which implies (5.13). That equalities (5.14) and (5.15) are equivalent to (5.13) is verified by a straightforward computation.

(ii) We need to check that

$$x_i^* = x_{i-1}\frac{x_i + y_i}{x_{i-1} + y_{i-1}}, \qquad y_i^* = y_i\frac{x_{i+1} + y_{i+1}}{x_i + y_i}, \tag{5.16}$$

where (x_i^*, y_i^*) are given by formulas (5.11) with S^- replaced by S and S by S^+.

The computation is simplified by the observation that

$$x_i + y_i = \frac{(S_{i+1}^- - S_i^-)(S_{i+2} - S_{i+1})}{(S_{i+1}^- - S_{i+2})(S_i^- - S_{i+1})}.$$

After substituting to (5.16), a direct computation reveals that the first of the equalities (5.16) is equivalent to the quotient of (5.14) and (5.15), whereas the second is equivalent to their product. □

The leapfrog transformation can be interpreted in terms of hyperbolic geometry. Let us identify $\mathbf{RP}^1$ with the circle at infinity of the hyperbolic plane $\mathbf{H}^2$. Then the restrictions of hyperbolic isometries on the circle at infinity are the projective transformations of $\mathbf{RP}^1$. Accordingly, S^- and S are ideal polygons in $\mathbf{H}^2$.

The projective transformation that interchanges the vertices S_{i-1} and S_{i+1} and fixes S_i is the reflection of the hyperbolic plane in the line L_i through S_i, perpendicular to the line $S_{i-1}S_{i+1}$ (that is, the altitude of the ideal triangle $S_{i-1}S_iS_{i+1}$); see Fig. 20 where we use the projective (Cayley–Klein) model of the hyperbolic plane.

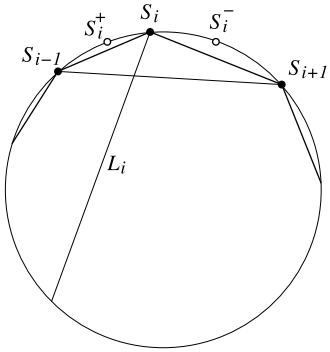

Fig. 20. Leapfrog transformation in the hyperbolic plane.

The ideal polygon obtained by reflecting each vertex S_i^- in the respective line L_i is S^+. Thus the leapfrog transformation Φ is presented as the composition of two involutions:

$$(S^-, S) \mapsto (S^+, S) \mapsto (S, S^+).$$

We note a certain similarity of the map Φ with the polygon recutting studied by Adler [2,3], which is also a completely integrable transformation of polygons (in the Euclidean plane or, more generally, Euclidean space). In Adler's case, one reflects the vertex V_i in the perpendicular bisector of the diagonal $V_{i-1}V_{i+1}$, after which one proceeds to the next vertex by increasing the index i by 1.

5.2.3. Lagrangian formulation of leapfrog transformation

The map Φ can be described as a discrete Lagrangian system. Let us recall relevant definitions, see, e.g., [46].

Given a manifold M, a Lagrangian system is a map $F : M \times M \to M \times M$ defined as follows:

$$F(x, y) = (y, z) \quad \text{if and only if} \quad \frac{\partial}{\partial y}\left(L(x, y) + L(y, z)\right) = 0,$$

where $L : M \times M \to \mathbf{R}$ is a function (called the Lagrangian).

Many familiar discrete time dynamical systems can be described this way (for example, the billiard ball map, for which $L(x, y) = |x-y|$ where x and y are points on the boundary of the billiard table).

Note that the map F does not change if the Lagrangian is changed as follows:

$$L(x, y) \mapsto L(x, y) + g(x) - g(y) \tag{5.17}$$

where g is an arbitrary function.

A Lagrangian system has an invariant pre-symplectic (that is, closed) differential 2-form

$$\omega = \sum_{i,j} \frac{\partial^2 L(x,y)}{\partial x_i \partial y_j} dx_i \wedge dy_j.$$

The form ω does not change under the transformation (5.17).

In the next proposition, assume that the n-gons in $\mathbf{RP}^1$ under consideration are closed (that is, the monodromy is the identity). As before, we choose an affine coordinate on the projective line and treat the vertices S_i and S_i^- as numbers. The index i is understood cyclically, so that $i = n+1$ is the same as $i = 1$.

Proposition 5.14. (i) *The leapfrog map Φ is a discrete Lagrangian system with the Lagrangian*

$$L(S^-, S) = \sum_i \ln|S_i - S_{i+1}| - \sum_i \ln|S_i - S_i^-|. \tag{5.18}$$

(ii) *The Lagrangian L changes under fractional–linear transformation*

$$x \mapsto \frac{ax+b}{cx+d}$$

as follows: $L(S^-, S) \mapsto L(S^-, S) + g(S^-) - g(S)$, where $g(S) = \sum_i \ln|cS_i + d|$.

Proof. (i) Differentiating $L(S^-, S) + L(S, S^+)$ with respect to S_i yields (5.13).

(ii) If $\bar{S} = (aS+b)/(cS+d)$ then

$$\bar{S}_i - \bar{S}_{i+1} = \frac{D(S_i - S_{i+1})}{(cS_i+d)(cS_{i+1}+d)}, \qquad \bar{S}_i - \bar{S}_i^- = \frac{D(S_i - S_i^-)}{(cS_i+d)(cS_i^-+d)}$$

with $D = ad - bc$. It follows that

$$\sum_i (\ln|\bar{S}_i - \bar{S}_{i+1}| - \ln|\bar{S}_i - \bar{S}_i^-|)$$
$$= \sum_i (\ln|S_i - S_{i+1}| - \ln|S_i - S_i^-)| + \sum_i (\ln|cS_i^- + d| - \ln|cS_i + d)|,$$

as claimed. □

Corollary 5.15. *The 2-form*

$$\omega = \sum_{i=1}^{n} \frac{dS_i^- \wedge dS_i}{(S_i^- - S_i)^2}.$$

is a closed $\mathrm{PGL}(2, \mathbf{R})$*-invariant differential form invariant under the map Φ.*

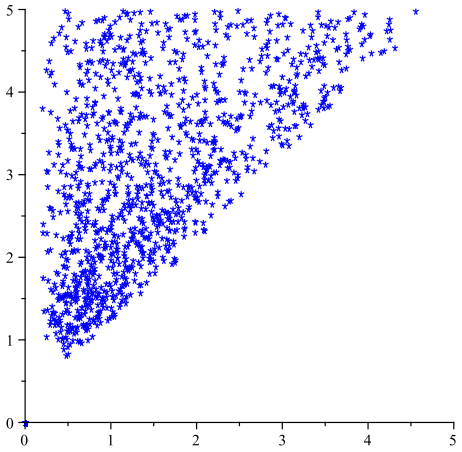

Fig. 21. Non-integrable behavior of the map Φ for $n = 6$.

We note that the form ω is not basic, that is, it does not descend on the quotient space $\mathcal{S}_n/PGL(2,\mathbf{R})$.

Remark 5.16. Numerical simulations show that Φ does not have integrable behavior. Fig. 21 shows chaotic behavior of two quantities: the horizontal axis is $S_2 - S_1$, the vertical axis is $S_3 - S_1$. Note that a chaotic-looking behavior of Φ does not contradict the integrability of T_2, since Φ is obtained from T_2 via a lifting that does not necessary preserve integrability.

5.2.4. Circle pattern

If the ground field is $\mathbf{C}$ then the mapping Φ can be interpreted as a certain circle pattern.

Consider Fig. 22. This figure depicts a local rule of constructing point S_i^+ from points S_{i-1}, S_i, S_{i+1} and S_i^-. Namely, draw the circle through points S_{i-1}, S_i^-, S_i, and then draw the circle through points S_i, S_{i+1}, tangent to the previous circle. Now repeat the construction: draw the circle through points S_{i+1}, S_i^-, S_i, and then draw the circle through points S_i, S_{i-1}, tangent to the previous circle. Finally, define S_i^+ to be the intersection point of the two "new" circles.

Proposition 5.17. *The tangency of two pairs of circles meeting at point S_i in Fig. 22 is equivalent to equations (5.13)–(5.15).*

Proof. A Möbius transformation sends a circle or a line to a circle or a line. Send point S_i to infinity; then the circles through this points become straight lines. Two circles are tangent if they make zero angle. Since Möbius transformations are conformal, the respective lines are parallel.

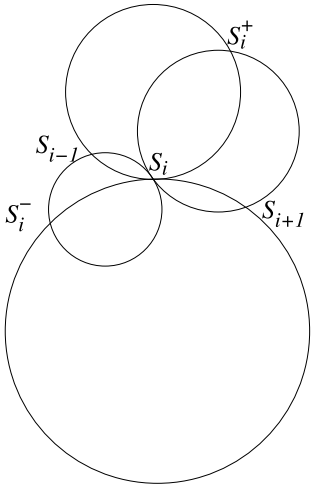

Fig. 22. Pairwise tangent circles.

Thus the configuration of circles in Fig. 22 becomes a parallelogram with vertices S_{i-1}, S_i^-, S_{i+1} and S_i^+. The quadrilateral is a parallelogram if and only if

$$S_{i-1} + S_{i+1} = S_i^- + S_i^+. \tag{5.19}$$

On the other hand, if $S_i = \infty$ then equation (5.14) becomes

$$\frac{S_i^+ - S_{i+1}}{S_i^- - S_{i-1}} = -1,$$

which is equivalent to (5.19). □

This circle pattern generalizes the one studied by O. Schramm in [35] in the framework of discretization of the theory of analytic functions (there the pairs of non-tangent neighboring circles were orthogonal). See also [4] concerning more general circle patterns with constant intersection angles and their relation with discrete integrable systems of Toda type.

Acknowledgments

It is a pleasure to thank the Hausdorff Research Institute for Mathematics whose hospitality the authors enjoyed in summer of 2011 where this research was initiated. We are grateful to A. Bobenko, V. Fock, S. Fomin, M. Glick, R. Kedem, R. Kenyon, B. Khesin, G. Mari-Beffa, V. Ovsienko, R. Schwartz, F. Soloviev, Yu. Suris for stimulating discussions and to the referee for valuable comments. M.G. was partially supported by the National Science Foundation grant DMS-1101462; M.S. was partially supported by the National Science Foundation grants DMS-1101369 and DMS-1362352; S.T. was

partially supported by the Simons Foundation grant No. 209361 and by the National Science Foundation grant DMS-1105442; A.V. was partially supported by the ISF grant No. 162/12.

Appendix A. Leapfrog map and Toda lattice (by Anton Izosimov[1])

The goal of this appendix is to explain the relation between the leapfrog map Φ and periodic Toda lattice. We show that the Toda flow may be obtained from the leapfrog map by first taking the continuous limit of the latter, and then reducing the resulting flow with respect to the natural $\mathrm{PGL}(2,\mathbf{R})$ action. This approach also gives a natural interpretation for three well-known compatible Poisson brackets associated with the Toda lattice.

A.1. Continuous limit of the leapfrog map and the Toda lattice

Denote by $\mathcal{R}_n(M)$ the space of twisted polygons in $\mathbf{RP}^1$ with monodromy M, where $M \in \mathrm{PGL}(2,\mathbf{R})$ is fixed. Let also $\mathcal{R}_n$ be the space of all twisted polygons: $\mathcal{R}_n = \bigsqcup_M \mathcal{R}_n(M)$; clearly, $\mathcal{R}_n$ and $\mathcal{P}_{2,n}$ defined in Section 5 are related via $\mathcal{P}_{2,n} = \mathcal{R}_n/\mathrm{PGL}(2,\mathbf{R})$. As in Section 5.2, let $\mathcal{S}_n$ denote the space of ordered pairs of twisted n-gons that have the same monodromy, i.e. $\mathcal{S}_n = \bigsqcup_M \mathcal{R}_n(M) \times \mathcal{R}_n(M)$.

Recall that the leapfrog map $\Phi\colon \mathcal{S}_n \to \mathcal{S}_n$ is defined as follows (see Section 5.2.2). Let $(S^-, S) \in \mathcal{S}_n$. For each $i \in \mathbf{Z}$, consider a projective involution $\sigma_i\colon \mathbf{RP}^1 \to \mathbf{RP}^1$ which fixes S_i and swaps S_{i-1} with S_{i+1}. Such an involution exists, and it is unique provided that the points S_{i-1}, S_i, S_{i+1} are pairwise distinct. Define a twisted n-gon S^+ by the rule $S_i^+ = \sigma_i(S_i^-)$, and set $\Phi(S^-, S) = (S, S^+)$.

It is natural to interpret the leapfrog map as a second order difference equation. Namely, assume that a twisted polygon $S \in \mathcal{R}_n$ depends on an additional variable $t \in h\mathbf{Z}$, where $h \in \mathbf{R}$ is a constant, and consider the equation

$$(S(t), S(t+h)) = \Phi(S(t-h), S(t)),$$

which is equivalent to

$$\frac{1}{S_i(t+h) - S_i(t)} + \frac{1}{S_i(t-h) - S_i(t)} = \frac{1}{S_{i+1}(t) - S_i(t)} + \frac{1}{S_{i-1}(t) - S_i(t)}, \tag{A.1}$$

cf. formula (5.13). Assuming that $S(t)$ is actually defined for all $t \in \mathbf{R}$ and taking the limit $h \to 0$ in equation (A.1), we obtain the following second order differential equation:

$$\frac{\ddot{S}_i}{\dot{S}_i^2} = \frac{1}{S_i - S_{i+1}} + \frac{1}{S_i - S_{i-1}}, \tag{A.2}$$

[1] Department of Mathematics, University of Toronto, Toronto, ON M5S 2E4, Canada. *E-mail address:* izosimov@math.utoronto.ca.

which we call the *leapfrog flow* (this equation, along with its discrete counterpart (A.1), appeared in [43,44]). The phase space of the leapfrog flow is

$$\hat{\mathrm{T}}\mathcal{R}_n = \bigsqcup_M \mathrm{T}\mathcal{R}_n(M) \subset \mathrm{T}\mathcal{R}_n,$$

where $\mathrm{T}\mathcal{R}_n$ stands for the tangent bundle of $\mathcal{R}_n$. This space $\hat{\mathrm{T}}\mathcal{R}_n$ has dimension $2n+3$ and should be regarded as a continuous analog of the space $\mathcal{S}_n$. Moreover, the space $\hat{\mathrm{T}}\mathcal{R}_n$ carries a natural $\mathrm{PGL}(2,\mathbf{R})$ action given by

$$S_i \mapsto \frac{aS_i+b}{cS_i+d}, \quad \dot{S}_i \mapsto \frac{ad-bc}{(cS_i+d)^2}\dot{S}_i.$$

Equation (A.2) is invariant with respect to this action, so it descends to the quotient space $\hat{\mathcal{T}}_n = (\hat{\mathrm{T}}\mathcal{R}_n)\,/\,\mathrm{PGL}(2,\mathbf{R})$. Let us take the functions

$$p_i = \frac{\dot{S}_i\dot{S}_{i+1}}{(S_{i+1}-S_i)^2}, \quad q_i = \frac{\dot{S}_i(S_{i+1}-S_{i-1})}{(S_{i+1}-S_i)(S_i-S_{i-1})} \tag{A.3}$$

as coordinates on the quotient.

Theorem A.1. *The image of the leapfrog flow (A.2) under the projection $\hat{\mathrm{T}}\mathcal{R}_n \to \hat{\mathcal{T}}_n$ is the periodic Toda lattice*

$$\begin{cases} \dot{p}_i = (q_i - q_{i+1})p_i, \\ \dot{q}_i = p_{i-1} - p_i, \end{cases} \tag{A.4}$$

where all indices are considered modulo n.

Proof. The proof is a straightforward computation (one needs to express equations (A.2) in terms of variables p_i, q_i). To identify (A.4) with the Toda lattice, introduce new variables (a_i, b_i) such that

$$p_i = a_i^2, \quad q_i = b_i. \tag{A.5}$$

In these coordinates, equations (A.4) become

$$\begin{cases} \dot{a}_i = \frac{1}{2}(b_i - b_{i+1})a_i, \\ \dot{b}_i = a_{i-1}^2 - a_i^2, \end{cases} \tag{A.6}$$

which is exactly the Toda system in Flaschka variables multiplied by the factor $-\frac{1}{2}$. □

Thus, we have obtained the Toda lattice from the leapfrog map by passing to the continuous limit, and then performing reduction. However, it is possible to go the other

way around and make the reduction first. Similarly to Section 5.2.2, we introduce the following functions on the space $\mathcal{S}_n = \{S^-, S\}$:

$$x_i = -[S_i^-, S_{i+1}^-, S_{i+2}^-, S_{i+1}], \quad y_i = x_i[S_{i+1}^-, S_{i+1}, S_{i+2}^-, S_{i+2}]. \tag{A.7}$$

The functions $x_1, \dots, x_n$, $y_1, \dots, y_n$ are invariant with respect to the $\mathrm{PGL}(2, \mathbf{R})$ action on $\mathcal{S}_n$. Moreover, they form a coordinate system on the quotient space $\mathcal{S}_n / \mathrm{PGL}(2, \mathbf{R})$. By descending the leapfrog map Φ to the quotient, we obtain the map T_2 given by (5.16). Again, assuming that $S_i = S_i(t)$ and $S_i^- = S_i(t-h)$, we get

$$x_i = 1 - hq_{i+1} + \dots, \quad y_i = h^2 p_{i+1} + \dots \tag{A.8}$$

where p, q variables are given by (A.3), and dots denote terms of higher order in h. Substituting expansions (A.8) into formula (5.16) for the map T_2 and taking the limit as $h \to 0$, we obtain the Toda lattice equations (A.4).

We summarize this discussion in the following commutative diagram:

$$\begin{array}{ccc} \text{Leapfrog map } \Phi & \xrightarrow[\text{reduction}]{\mathrm{PGL}(2,\mathbf{R})} & \text{Map } T_2 \\ \Big\downarrow \text{Continuous limit } h \to 0 & & \Big\downarrow \text{Continuous limit } h \to 0 \\ \text{Leapfrog flow (A.2)} & \xrightarrow[\text{reduction}]{\mathrm{PGL}(2,\mathbf{R})} & \text{Periodic Toda lattice.} \end{array} \tag{A.9}$$

In the next two sections we show that the horizontal arrows in this diagram are Poisson maps, provided that we confine ourselves to closed polygons (see the diagram at the end of the last section below).

Remark A.2. The relation between discrete-time system (A.1) and its continuous-time counterpart (A.2) to the Toda lattice was described in [43,44] as a Bäcklund-type transformation. Here we put this relation in the context of Hamiltonian reduction.

A.2. Hamiltonian structure of the leapfrog flow and the cubic Toda bracket

In this section, we show that the leapfrog flow restricted to closed polygons is Hamiltonian, and that the corresponding Poisson structure gives rise to the cubic bracket for the Toda lattice.

First, we note that the tangent bundle of any one-dimensional manifold carries a natural quadratic Poisson structure. Indeed, let M be a one-dimensional manifold, and let $\langle , \rangle$ be any Riemannian metric on M. Then the formula

$$v \to \frac{\langle v, w\rangle}{\langle v, v\rangle}$$

defines a diffeomorphism $\mathrm{T}M \setminus M \to \mathrm{T}^*M \setminus M$, which does not depend on the choice of the metric. Therefore, there is a canonical Poisson structure on $\mathrm{T}M$. It is explicitly given by

$$\{\dot{x}, x\} = \dot{x}^2.$$

Now consider the space $\mathcal{R}_n(\mathrm{Id})$ of closed n-gons. We have $\mathcal{R}_n(\mathrm{Id}) = \left(\mathbf{RP}^1\right)^n$, so $\mathrm{T}\mathcal{R}_n(\mathrm{Id}) = \left(\mathrm{T}\mathbf{RP}^1\right)^n$, and the tangent bundle to $\mathcal{R}_n(\mathrm{Id})$ carries a Poisson structure given by

$$\{\dot{S}_i, S_i\} = \dot{S}_i^2. \tag{A.10}$$

This Poisson structure is canonical in the following sense: it is invariant with respect to any "componentwise" transformations of the form $S_i \mapsto f_i(S_i)$; $\dot{S}_i \mapsto f_i'(S_i)\dot{S}_i$.

Proposition A.3. *The leapfrog flow (A.2) restricted to closed polygons is Hamiltonian with respect to the canonical Poisson structure (A.10).*

Proof. The Hamiltonian function is given by $H = \sum_{i=1}^n \left(\ln(S_i - S_{i-1}) - \ln \dot{S}_i\right)$, where $S_0 = S_n$. □

The image of $\mathrm{T}\mathcal{R}_n(\mathrm{Id})$ under the projection $\pi\colon \hat{\mathrm{T}}\mathcal{R}_n \to \hat{\mathcal{T}}_n$ is a submanifold of codimension 3. The action of $\mathrm{PGL}(2, \mathbf{R})$ on $\mathrm{T}\mathcal{R}_n(\mathrm{Id})$ preserves the canonical bracket, therefore this bracket descends to $\pi(\mathrm{T}\mathcal{R}_n(\mathrm{Id}))$.

Theorem A.4. 1. *The image of the canonical bracket (A.10) on the space of closed polygons under the projection* $\mathrm{T}\mathcal{R}_n(\mathrm{Id}) \to \mathcal{T}_n(\mathrm{Id}) = (\mathrm{T}\mathcal{R}_n(\mathrm{Id}))\,/\,\mathrm{PGL}(2, \mathbf{R})$ *is given by*

$$\begin{aligned} &\{p_i, p_{i+1}\} = 2p_ip_{i+1}q_{i+1}, \quad \{q_i, q_{i+1}\} = p_i(q_i + q_{i+1}), \quad \{p_i, q_{i-1}\} = -p_ip_{i-1}, \\ &\{p_i, q_i\} = -p_i^2 - p_iq_i^2, \quad \{p_i, q_{i+1}\} = p_i^2 + p_iq_{i+1}^2, \quad \{p_i, q_{i+2}\} = p_ip_{i+1}. \end{aligned} \tag{A.11}$$

2. *Formulas (A.11) define a Poisson bracket on the whole space* $\hat{\mathcal{T}}_n$.

Proof. The first statement is proved by a straightforward computation, so let us prove the second statement. It suffices to show that (A.11) satisfies Jacobi identities. Note that these identities are of the following "local" form:

$$F(p_{i-k}, \dots, p_{i+k}, q_{i-k}, \dots, q_{i+k}) = 0,$$

where k is some constant. Also note that since this bracket is obtained from bracket (A.10) by Poisson reduction, it automatically satisfies the Jacobi identity on the codimension 3 submanifold $\mathcal{T}_n(\mathrm{Id}) \subset \hat{\mathcal{T}}_n$. Therefore, the polynomial F should vanish on

closed polygons. However, the condition of being closed is not local, so F must vanish identically. □

In Flaschka variables (a_i, b_i) given by (A.5), bracket (A.11) reads

$$\{a_i, a_{i+1}\} = \frac{1}{2}a_i a_{i+1} b_{i+1}, \quad \{b_i, b_{i+1}\} = a_i^2(b_i + b_{i+1}), \quad \{a_i, b_{i-1}\} = -\frac{1}{2}a_i a_{i-1}^2,$$
$$\{a_i, b_i\} = -\frac{1}{2}(a_i^3 + a_i b_i^2), \quad \{a_i, b_{i+1}\} = \frac{1}{2}(a_i^3 + a_i b_{i+1}^2),$$
$$\{a_i, b_{i+2}\} = \frac{1}{2}a_i a_{i+1}^2. \tag{A.12}$$

The latter bracket coincides with the cubic Poisson structure for the Toda lattice. Accordingly, we can interpret the upper horizontal arrow in diagram (A.9) as Hamiltonian reduction, provided that we confine ourselves to closed polygons. In the next section, we show that a similar interpretation exists for the lower horizontal arrow.

Remark A.5. Cubic Poisson bracket (A.12) for the Toda lattice was found in [26]. The derivation of the cubic Toda bracket from a trigonometric analog of the system (A.2) can be found in [43]. The group-theoretic meaning of that derivation is unknown.

Remark A.6. Note that the action of the group $\mathrm{PGL}(2, \mathbf{R})$ on $\mathrm{T}\mathcal{R}_n(\mathrm{Id})$ is Hamiltonian. The corresponding moment map $\mathrm{T}\mathcal{R}_n(\mathrm{Id}) \to \mathfrak{sl}(2, \mathbf{R})^*$ is given by the functions

$$e = \sum_{i=1}^{n} \frac{1}{\dot{S}_i}, \quad h = 2\sum_{i=1}^{n} \frac{S_i}{\dot{S}_i}, \quad f = -\sum_{i=1}^{n} \frac{S_i}{\dot{S}_i}$$

satisfying canonical $\mathfrak{sl}(2)$ relations $\{e, f\} = h$, $\{h, e\} = 2e$, and $\{h, f\} = -2f$. This in particular implies that the only Casimir of the cubic Toda bracket (A.11) on $\mathcal{T}_n(\mathrm{Id})$ is obtained by descending the $\mathfrak{sl}(2)$ Casimir

$$C = \frac{1}{4}h^2 + ef = \sum_{i<j} \frac{(S_i - S_j)^2}{\dot{S}_i \dot{S}_j},$$

and thus the Poisson manifold $\mathcal{T}_n(\mathrm{Id})$ is foliated into symplectic leaves that are generically of codimension 1. We do not know whether the function C extends to a Casimir of the cubic Toda bracket on the ambient Poisson manifold $\hat{\mathcal{T}}_n$. It is also an interesting question whether there exists a $\mathrm{PGL}(2, \mathbf{R})$ invariant Poisson bracket on the whole space $\hat{\mathrm{T}}\mathcal{R}_n$ that descends to the cubic Toda bracket.

A.3. Tri-Hamiltonian structure of the map T_2

As it was shown in Section 5.2.3, the leapfrog map Φ restricted to closed polygons preserves the closed 2-form

$$\Omega = \sum_{i=1}^{n} \frac{\mathrm{d}S_i \wedge \mathrm{d}S_i^-}{(S_i - S_i^-)^2}.$$

Therefore, it preserves the Poisson structure Ω^{-1} given by

$$\{S_i, S_i^-\} = (S_i - S_i^-)^2. \tag{A.13}$$

This is a discrete version of the bracket (A.10). Bracket (A.13) is not canonical, however it is still invariant with respect to the $\mathrm{PGL}(2, \mathbf{R})$ action.

Theorem A.7. 1. *The image of the bracket* (A.13) *under the projection* $\mathcal{R}_n(\mathrm{Id}) \times \mathcal{R}_n(\mathrm{Id}) \to (\mathcal{R}_n(\mathrm{Id}) \times \mathcal{R}_n(\mathrm{Id}))/\mathrm{PGL}(2, \mathbf{R})$ *is the bracket* $\{\,,\}_3$ *given by*

$$\begin{aligned}
\{x_i, x_{i+1}\}_3 &= y_i(1 - x_i x_{i+1}), \quad \{y_i, y_{i+1}\}_3 = y_i y_{i+1}(2 - 2x_{i+1} - y_i - y_{i+1}),\\
\{x_i, y_{i-2}\}_3 &= x_i y_{i-1} y_{i-2}, \quad \{x_i, y_{i+1}\}_3 = -x_i y_i y_{i+1},\\
\{x_i, y_{i-1}\}_3 &= x_i y_{i-1}^2 + y_{i-1}(x_i - 1)^2, \quad \{x_i, y_i\}_3 = -x_i y_i^2 - y_i(x_i - 1)^2,
\end{aligned} \tag{A.14}$$

where (x, y) *are coordinates on* $\mathcal{S}_n / \mathrm{PGL}(2, \mathbf{R})$ *defined by* (A.7).

2. *Formulas* (A.14) *define a Poisson bracket on the whole space* $\mathcal{S}_n / \mathrm{PGL}(2, \mathbf{R})$. *This bracket is preserved by the map* T_2.

Proof. The proof is analogous to the proof of Theorem A.4. □

Recall that Poisson brackets are called compatible if their arbitrary linear combination is itself a Poisson bracket.

Corollary A.8. *(Cf. [43].) The map* T_2 *is tri-Hamiltonian: it preserves three compatible Poisson brackets given by*

$$\begin{aligned}
\{x_i, x_{i+1}\}_1 &= y_i, \quad \{x_i, y_{i-1}\}_1 = y_{i-1}, \quad \{x_i, y_i\}_1 = -y_i,\\
\{y_i, y_{i+1}\}_2 &= y_i y_{i+1}, \quad \{x_i, y_{i-1}\}_2 = -x_i y_{i-1}, \quad \{x_i, y_i\}_2 = x_i y_i,\\
\{x_i, x_{i+1}\}_{3'} &= -y_i x_i x_{i+1}, \quad \{y_i, y_{i+1}\}_{3'} = -y_i y_{i+1}(2x_{i+1} + y_i + y_{i+1}),\\
\{x_i, y_{i-2}\}_{3'} &= x_i y_{i-1} y_{i-2}, \quad \{x_i, y_{i-1}\}_{3'} = x_i y_{i-1}^2 + y_{i-1} x_i^2,\\
\{x_i, y_i\}_{3'} &= -x_i y_i^2 - y_i x_i^2, \quad \{x_i, y_{i+1}\}_{3'} = -x_i y_i y_{i+1}.
\end{aligned}$$

Proof. First, let us prove that $\{\,,\}_1$, $\{\,,\}_2$, $\{\,,\}_{3'}$ are compatible Poisson brackets. Let Π denote the Poisson tensor corresponding to the bracket (A.14). Represent Π as $\Pi = \Pi_3 + \Pi_2 + \Pi_1$ where Π_3, Π_2, Π_1 are homogeneous cubic, quadratic, and linear tensors respectively. Note that the bracket corresponding to Π_1 is $\{\,,\}_1$, the bracket corresponding to Π_2 is $2\{\,,\}_2$, and the bracket corresponding to Π_3 is $\{\,,\}_{3'}$. Therefore, to

prove that $\{\,,\}_1$, $\{\,,\}_2$, $\{\,,\}_{3'}$ are compatible Poisson brackets, it suffices to show that Π_1, Π_2, Π_3 are compatible Poisson tensors.

Since Π is Poisson, we have $[\Pi,\Pi]=0$ where $[\,,]$ is the Schouten–Nijenhuis bracket. This yields

$$[\Pi_3,\Pi_3]=0,\quad [\Pi_2,\Pi_3]=0,\quad [\Pi_2,\Pi_2]+[\Pi_1,\Pi_3]=0,$$
$$[\Pi_1,\Pi_2]=0,\quad [\Pi_1,\Pi_1]=0. \tag{A.15}$$

Further, we have $[\Pi_2,\Pi_2]=0$. Indeed, the bracket corresponding to Π_2 is

$$\{y_i,y_{i+1}\}=2y_iy_{i+1}\quad \{x_i,y_{i-1}\}=-2x_iy_{i-1},\quad \{x_i,y_i\}=2x_iy_i.$$

This bracket is obviously Poisson: it becomes constant in coordinates $(\ln x_i,\ln y_i)$ (also note that up to a factor -2 this bracket coincides with (4.7)). So, $[\Pi_2,\Pi_2]=0$. Together with identities (A.15), the latter implies that the tensors Π_1, Π_2, and Π_3 are compatible Poisson tensors.

To prove that the brackets $\{\,,\}_1$, $\{\,,\}_2$, $\{\,,\}_{3'}$ are preserved by the map T_2, note that this map is homogeneous of degree one. Therefore, since T_2 preserves the bracket (A.14), it also preserves its homogeneous components Π_3, Π_2, Π_1. □

Remark A.9. Note that we cannot use the same trick to recover linear and quadratic Poisson brackets for the Toda lattice from the cubic one. Indeed, the proof of Corollary A.8 relies on the existence of coordinates x_i,y_i in which the map T_2 is homogeneous, while the bracket (A.14) is not. To apply the same argument for the Toda lattice, we should pass to Flaschka variables (a_i,b_i) where equations of motion take the homogeneous form (A.8). However, the cubic bracket in this coordinates is also homogeneous (A.12). For this reason, it is not possible to extract the linear and quadratic bracket from the cubic one; linear and quadratic Poisson structures manifest themselves in a cubic structure at the discrete level only.

Nevertheless, it is possible to construct compatible Poisson brackets for the Toda lattice by taking continuous limit of the brackets described in Corollary A.8. Using formulas (A.8), we have

$$\lim_{h\to 0}\frac{1}{h}\{\,,\}_3=\{\,,\}_3^T,\quad \lim_{h\to 0}(\{\,,\}_2+\{\,,\}_1)=\{\,,\}_2^T,\quad \lim_{h\to 0}h\{\,,\}_1=\{\,,\}_1^T,$$

where $\{\,,\}_1^T$, $\{\,,\}_2^T$, $\{\,,\}_3^T$ are, respectively, linear, quadratic, and cubic Toda brackets. Note that homogeneous brackets $\{\,,\}_{3'}$ and $\{\,,\}_2$ do not have well-defined continuous limits.

Remark A.10. Homogeneous Poisson brackets $\{\,,\}_1$, $\{\,,\}_2$, and $\{\,,\}_{3'}$ appeared in [6] as compatible Poisson structures for relativistic Toda lattice.

We summarize our discussion in the following "Poisson" version of diagram (A.9):

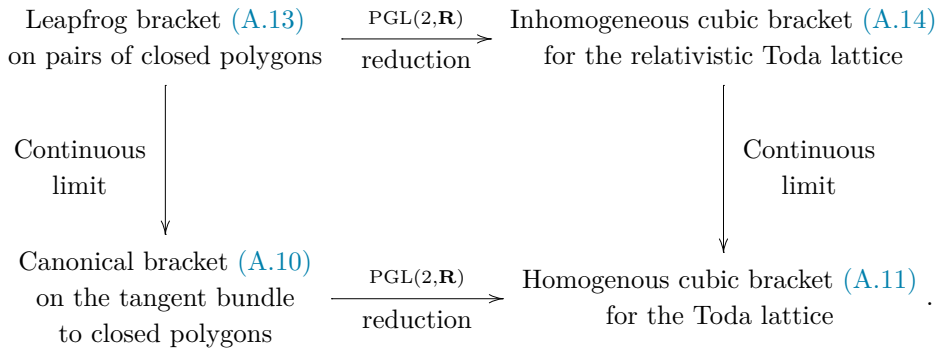

References

[1] M. Adams, J. Harnad, J. Hurtubise, Dual moment maps into loop algebras, Lett. Math. Phys. 20 (1990) 299–308.
[2] V. Adler, Cutting of polygons, Funct. Anal. Appl. 27 (1993) 141–143.
[3] V. Adler, Integrable deformations of a polygon, Phys. D 87 (1995) 52–57.
[4] A. Bobenko, T. Hoffmann, Hexagonal circle patterns and integrable systems: patterns with constant angles, Duke Math. J. 116 (2003) 525–566.
[5] H. Busemann, P. Kelly, Projective Geometry and Projective Metrics, Academic Press, New York, 1953.
[6] P. Damianou, Multiple Hamiltonian structures for Toda-type systems, J. Math. Phys. 35 (1994) 5511–5541.
[7] B. Dubrovin, I. Krichever, S. Novikov, Integrable systems. I, Dynamical systems. IV, Encyclopaedia Math. Sci., vol. 4, Springer, Berlin, 2001, pp. 177–332.
[8] L. Faddeev, L. Takhtajan, Hamiltonian Methods in the Theory of Solitons, Springer-Verlag, Berlin, 1987.
[9] V. Fock, A. Marshakov, Loop groups, clusters, dimers and integrable systems, preprint, arXiv:1401.1606.
[10] S. Fomin, A. Zelevinsky, Cluster algebras. IV. Coefficients, Compos. Math. 143 (2007) 112–164.
[11] M. Gekhtman, M. Shapiro, S. Tabachnikov, A. Vainshtein, Higher pentagram maps, weighted directed networks, and cluster dynamics, Electron. Res. Announc. Math. Sci. 19 (2012) 1–17.
[12] M. Gekhtman, M. Shapiro, A. Vainshtein, Poisson geometry of directed networks in a disk, Selecta Math. 15 (2009) 61–103.
[13] M. Gekhtman, M. Shapiro, A. Vainshtein, Cluster Algebras and Poisson Geometry, Amer. Math. Soc., Providence, RI, 2010.
[14] M. Gekhtman, M. Shapiro, A. Vainshtein, Generalized Bäcklund–Darboux transformations for Coxeter–Toda flows from a cluster algebra perspective, Acta Math. 206 (2011) 245–310.
[15] M. Gekhtman, M. Shapiro, A. Vainshtein, Poisson geometry of directed networks in an annulus, J. Eur. Math. Soc. (JEMS) 14 (2012) 541–570.
[16] M. Glick, The pentagram map and Y-patterns, Adv. Math. 227 (2011) 1019–1045.
[17] M. Glick, On singularity confinement for the pentagram map, J. Algebraic Combin. 38 (2013) 597–635.
[18] M. Glick, The Devron property, J. Geom. Phys. 87 (2015) 161–189.
[19] A. Goncharov, R. Kenyon, Dimers and cluster integrable systems, Ann. Sci. Éc. Norm. Supér. 46 (2013) 747–813.
[20] T. Kato, A note on the pentagram map and tropical geometry, preprint, arXiv:1405.0084.
[21] R. Kedem, P. Vichitkunakorn, T-systems and the pentagram map, J. Geom. Phys. 87 (2015) 233–247.
[22] B. Khesin, F. Soloviev, The pentagram map in higher dimensions and KdV flows, Electron. Res. Announc. Math. Sci. 19 (2012) 86–96.

[23] B. Khesin, F. Soloviev, Integrability of a space pentagram map, Math. Ann. 357 (2013) 1005–1047.
[24] B. Khesin, F. Soloviev, Non-integrability vs. integrability in pentagram maps, J. Geom. Phys. 87 (2015) 275–285.
[25] B. Khesin, F. Soloviev, The geometry of dented pentagram maps, J. Eur. Math. Soc. (JEMS) 18 (2016) 147–179.
[26] B. Kupershmidt, Discrete Lax equations and differential-difference calculus, Astérisque 123 (1985) 1–212.
[27] G. Mari Beffa, On generalizations of the pentagram map: discretizations of AGD flows, J. Nonlinear Sci. 23 (2013) 303–334.
[28] G. Mari Beffa, On integrable generalizations of the pentagram map, Int. Math. Res. Not. IMRN (2015) 3669–3693.
[29] J. Moser, A.P. Veselov, Discrete versions of some classical integrable systems and factorization of matrix polynomials, Comm. Math. Phys. 139 (1991) 217–243.
[30] M. Olshanetsky, A. Perelomov, A. Reyman, M. Semenov-Tian-Shansky, Integrable systems. II, Dynamical systems. VII, Encyclopaedia Math. Sci., vol. 16, Springer, Berlin, 1994, pp. 83–259.
[31] V. Ovsienko, R. Schwartz, S. Tabachnikov, Quasiperiodic motion for the Pentagram map, Electron. Res. Announc. Math. Sci. 16 (2009) 1–8.
[32] V. Ovsienko, R. Schwartz, S. Tabachnikov, The Pentagram map: a discrete integrable system, Comm. Math. Phys. 299 (2010) 409–446.
[33] V. Ovsienko, R. Schwartz, S. Tabachnikov, Liouville–Arnold integrability of the pentagram map on closed polygons, Duke Math. J. 162 (2013) 2149–2196.
[34] A. Postnikov, Total positivity, Grassmannians, and networks, preprint, arXiv:math.CO/0609764.
[35] O. Schramm, Circle patterns with the combinatorics of the square grid, Duke Math. J. 86 (1997) 347–389.
[36] R. Schwartz, The pentagram map, Exp. Math. 1 (1992) 71–81.
[37] R. Schwartz, The pentagram map is recurrent, Exp. Math. 10 (2001) 519–528.
[38] R. Schwartz, Discrete monodromy, pentagrams, and the method of condensation, J. Fixed Point Theory Appl. 3 (2008) 379–409.
[39] R. Schwartz, The pentagram integrals for Poncelet families, J. Geom. Phys. 87 (2015) 432–449.
[40] R. Schwartz, S. Tabachnikov, Elementary surprises in projective geometry, Math. Intelligencer 32 (3) (2010) 31–34.
[41] R. Schwartz, S. Tabachnikov, The Pentagram integrals on inscribed polygons, Electron. J. Combin. 18 (2011) P171.
[42] F. Soloviev, Integrability of the pentagram map, Duke Math. J. 162 (2013) 2815–2853.
[43] Yu. Suris, On some integrable systems related to the Toda lattice, J. Phys. A 30 (6) (1997) 2235–2249.
[44] Yu. Suris, The Problem of Integrable Discretization: Hamiltonian Approach, Springer-Verlag, Berlin, 2003.
[45] K. Talaska, Determinants of weighted path matrices, preprint, arXiv:1202.3128.
[46] A. Veselov, Integrable mappings, Russian Math. Surveys 46 (1991) 1–51.